Analytical, numerical and experimental study of the finite inflation of circular membranes

Matteo Pelliciari[a,b,*], Stefano Sirotti[b,a], Angelo Aloisio[c], Angelo Marcello Tarantino[a]

[a] *DIEF, Department of Engineering "Enzo Ferrari", via P. Vivarelli 10, 41125 Modena, Italy*
[b] *College of Civil Engineering, Fuzhou University, No. 2 Xue Yuan Road, 350108 Fuzhou, Fujian Province, PR China*
[c] *Department of Civil, Construction-Architectural and Environmental Engineering, University of l'Aquila, via G. Gronchi 18, 67100 L'Aquila, Italy*

Abstract

In the present work we derive an analytical expression for the pressure-deflection curve of circular membranes subjected to inflation. This problem has been studied mostly from a numerical point of view and there is still a lack of accurate closed-form solutions in nonlinear elasticity. The analytical formulation is developed with a semi-inverse method by setting a priori the kinematics of deformation of the membrane. A compressible Mooney-Rivlin material model is considered and a pressure-deflection relation is derived from the equilibrium. The kinematics is approximated and therefore the obtained solution is not exact. Consequently, the formulation is adjusted by introducing an additional polynomial function in the pressure-deflection equation. The polynomial is calibrated by fitting numerical solutions of the exact system of differential equilibrium equations. The calibration is done over a wide range of constitutive parameters that covers the response of all rubber materials for technological applications. As a result, a definitive and accurate expression of the applied pressure as a function of the deflection of the membrane is obtained. The formula is validated with finite element (FE) simulations and compared with other solutions available in the literature. The comparison shows that the present model is more accurate. In addition, unlike the other models, it can be applied to compressible materials. Experimental uniaxial and bulge tests are carried out on rubber materials and the model proposed is used to characterize the Mooney-Rivlin constitutive parameters. Since the pressure-deflection formula is accurate and easy-to-use, it is an innovative tool in engineering applications of inflated membranes.

Keywords: Inflated membrane; Analytical solution; Mooney-Rivlin material; Nonlinear elasticity; Experimental mechanics

1. Introduction

The equilibrium of initially flat circular membranes subjected to uniform lateral pressure is a benchmark problem in nonlinear elasticity. Since the pioneering works by Treloar [1] and Adkins and Rivlin [2], many researchers focused on this problem.

The scientific interest towards this topic is driven by the numerous applications in various fields of engineering. Because of their capability of withstanding large deformations, rubber membranes are used in soft robotics [3–5], flexible electronics [6, 7], dielectric systems [8–12], aerodynamics [13] and nano devices [14, 15]. Models for the inflation of membranes are often applied in biomechanics. For instance, Wineman et al. [16] considered the membrane inflation for the material identification of soft tissue and Serina et al. [17] modeled the human fingertip pulp as an inflated membrane in finite elasticity. Structural engineering

*Corresponding author. Tel.: +39 3334858333.
Email addresses: matteo.pelliciari@unimore.it (Matteo Pelliciari), stefano.sirotti@unimore.it (Stefano Sirotti), angelo.aloisio1@univaq.it (Angelo Aloisio), angelomarcello.tarantino@unimore.it (Angelo Marcello Tarantino)

also sees many important applications of membrane structures. This mainly because they are very light and load adaptive, minimizing thus the variation of stress states when subjected to external loads. They allow to cover large spans with a minimal use of materials [18, 19]. These systems are therefore of primary importance for applications in terrestrial and space structures [20, 21]. Applications in the nonlinear flexural response of composite panel structures are also of great importance [22–27].

Rubber membranes undergo large deformations when subjected to inflation. Hence, material and geometrical nonlinearities play an important role, resulting in a complex mechanical behavior. Indeed, an exact closed-form solution to the problem of inflation of circular membranes does not exist, not even for the simplest case of linearly elastic material [28]. Due to the above reasons, this problem has been investigated mostly from a numerical point of view. To this regard, Yang and Feng [29] managed to transform the boundary-value equilibrium problem into an initial value problem. In this way, the solution can be obtained by standard numerical methods for integrating ordinary differential equations. Since this breakthrough work, many other authors used this numerical approach to solve more complex problems. DasGupta and Patil [30] and Chaudhuri and DasGupta [31] investigated the finite inflation of pre-stretched hyperelastic circular membranes assuming an isotropic and incompressible Mooney-Rivlin material model. Liu et al. [32] and Patil et al. [33] analyzed the contact mechanics of inflated membranes considering various interface conditions. Also in these works the authors assumed an incompressible Mooney-Rivlin law for the material. Other numerical solutions to problems involving the inflation of hyperelastic rubber membranes can be found in [34–41].

Analytical solutions are necessary for straightforward and direct predictions of the mechanical response of inflated membranes. To give an idea of the importance of analytical solutions we recall that experiments on inflated membranes are a useful tool for the characterization of the material behavior [42]. It is widely known that, especially when dealing with large deformations, the parameters of the material model should not be determined considering only uniaxial stress states [43–45]. In this regard, bulge tests are the easiest way of reproducing biaxial states of stress to be used for the identification of the material parameters [46]. However, with only numerical solutions available, the estimation of the material parameters that fit the experiments is complex and time consuming.

Due to the complexity of the equilibrium problem of circular inflated membranes, only a few analytical solutions were proposed. Strong simplifying assumptions were made to derive such solutions. Fichter [28] derived a solution in the form of a truncated power series assuming that the deformations are small. Coelho et al. [47] extended the Fichter's solution considering large deformations, but the hypothesis of linearly elastic constitutive behavior was maintained. This does not reflect the behavior of real solids subjected to large deformations. Hence, Yuan et al. [48] abandoned the hypothesis of linearly elastic behavior and considered a Mooney-Rivlin material. However, the authors assumed that the profile of deformation of the inflated membrane is a spherical cap, which is not always the case. In addition, they assumed that the membrane undergoes equibiaxial stretching during inflation. This simplifies significantly the theoretical formulation. Another solution was derived by Yang et al. [49] for pre-stretched flat circular membranes composed of neo-Hookean material. Since the membrane is pre-stretched, the authors assumed that the stretches are very large and thus neglected some terms in the equilibrium equations. It is clear that this solution is only valid when stretches are very large and only for rubber materials that can be simulated with a neo-Hookean law, which has a rather restricted validity. We recall that, apart from the works that consider a linearly elastic behavior, in all the above works it is assumed that the material is incompressible. This assumption has not a general validity and may thus be inaccurate in certain cases [50].

In the present work, we derive an analytical solution for the inflation of circular hyperelastic membranes composed of compressible Mooney-Rivlin material. The formulation is developed in the context of finite elasticity, considering both large deformations and material nonlinearity. Firstly, we assume that the flat undeformed membrane transforms into a spherical cap. On the basis of this assumption, we derive an expression for the applied pressure as a function of the deflection of the membrane. As already mentioned, the hypothesis that the membrane deforms into a spherical cap is not always accurate and does not give an exact analytical solution. Therefore, we adopt the numerical solution proposed by Yang and Feng [29] and we carry out simulations varying the material parameters. The range of material parameters considered covers the behavior of all rubbers used in technological applications. Consequently, we adjust a posteriori

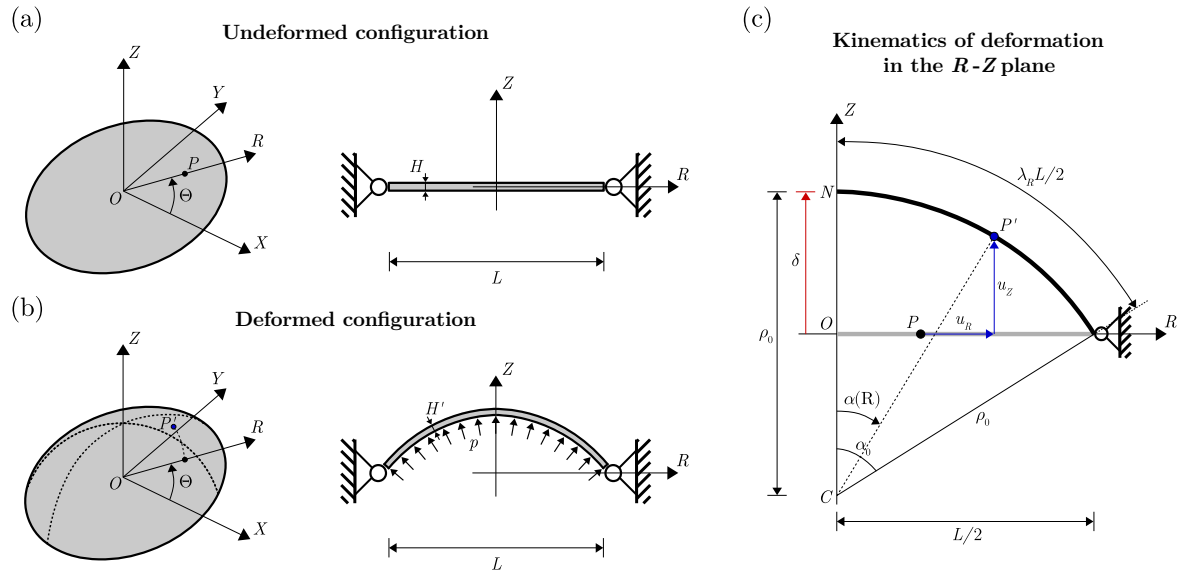

Figure 1: Circular membrane subjected to uniform lateral pressure p. Representation of (a) undeformed and (b) deformed configurations, where L is the diameter, H is the initial thickness and H' is the thickness after deformation. Material point P with cylindrical coordinates $(R,\Theta,0)$ moves to P', with coordinates (R',Θ,Z'). The membrane is axisymmetric and therefore the kinematics of deformation is described in the R-Z plane, as shown in (c). It is assumed that the initially flat membrane transforms into a spherical cap with central angle $2\alpha_0$ and radius ρ_0. The deflection of the central point of the membrane is denoted with δ.

our model by introducing an additional polynomial function in the pressure-deflection equation. As a result, we obtain an accurate expression for the pressure-deflection response of circular membranes composed of compressible Mooney-Rivlin material. Note that the solution that we propose is not exact, but it is based on a simplified analytical model which is adjusted by fitting numerical results. This approach allows us to derive an accurate formulation that can be employed for practical applications.

The pressure-deflection formula is validated with FE simulations and compared with other solutions from the literature, showing its advantages. After validation, we carry out experiments on three kinds of rubber. Uniaxial tensile tests and bulge tests are presented. We demonstrate the effectiveness of the proposed formula, especially for what concerns the characterization of rubber materials. Differently from the other solutions in the literature, the model presented in this work can be applied to compressible materials. Furthermore, the comparison with solutions proposed by other authors shows that our model gives a more accurate prediction of the pressure-deflection curve.

2. Analytical model for circular inflated membranes

In this section we derive a pressure-deflection relation for circular membranes under uniform lateral pressure. Firstly, we describe the kinematics of deformation by assuming that the flat undeformed membrane transforms into a spherical cap. Consequently, a compressible Mooney-Rivlin material law is considered and the equilibrium equation is derived. From the equilibrium equation, the expression of the applied pressure as a function of the deflection is obtained.

We consider a circular membrane with diameter L and thickness H. As shown in Fig. 1(a), the membrane is initially flat. We define a cylindrical material coordinate system (R,Θ,Z) with origin in O. After inflation, the membrane is subjected to the uniformly distributed pressure p and the generic material point P moves to P', with coordinates (R',Θ,Z'). It is assumed that the flat membrane transforms into a spherical cap. Although this assumption has been widely employed in the literature [48], it is well-known that in general

it does not provide an exact description of the kinematics of inflated membranes. However, we will base our model on such assumption and we will correct the formulation a posteriori by fitting numerical simulations.

Under the aforementioned assumption, the membrane deforms according to the kinematics of Fig. 1(c). The displacement field of material point P with coordinates $(R,\Theta,0)$ reads

$$\begin{cases} u_R(P) = R' - R = \rho_0 \sin\alpha(R) - R, \\ u_\Theta(P) = 0, \\ u_Z(P) = Z' = \rho_0 \left[\cos\alpha(R) - \cos\alpha_0\right], \end{cases} \tag{1}$$

with $\alpha_0 \in (0,\pi)$ and

$$\rho_0 = \frac{L}{2\sin\alpha_0}, \qquad \alpha(R) = \frac{2\alpha_0 R}{L}. \tag{2}$$

Hereinafter, the dependence of angle α to the radial coordinate R will be omitted for the sake of simplicity. The cylindrical components of deformation vector $\boldsymbol{\varphi}(P)$ are

$$\begin{cases} \varphi_R(P) = \rho_0 \sin\alpha, \\ \varphi_\Theta(P) = \Theta, \\ \varphi_Z(P) = \rho_0 \left(\cos\alpha - \cos\alpha_0\right). \end{cases} \tag{3}$$

The gradient of the deformation vector expressed in cylindrical coordinates is

$$[\nabla\boldsymbol{\varphi}] = \begin{bmatrix} \dfrac{\partial\varphi_R}{\partial R} & \dfrac{1}{R}\dfrac{\partial\varphi_R}{\partial\Theta} & \dfrac{\partial\varphi_R}{\partial Z} \\ \varphi_R\dfrac{\partial\varphi_\Theta}{\partial R} & \dfrac{\varphi_R}{R}\dfrac{\partial\varphi_\Theta}{\partial\Theta} & \varphi_R\dfrac{\partial\varphi_\Theta}{\partial Z} \\ \dfrac{\partial\varphi_Z}{\partial R} & \dfrac{1}{R}\dfrac{\partial\varphi_Z}{\partial\Theta} & \dfrac{\partial\varphi_Z}{\partial Z} \end{bmatrix} = \begin{bmatrix} \rho_0\dfrac{\partial\alpha}{\partial R}\cos\alpha & 0 & 0 \\ 0 & \dfrac{\rho_0\sin\alpha}{R} & 0 \\ -\rho_0\dfrac{\partial\alpha}{\partial R}\sin\alpha & 0 & 0 \end{bmatrix}. \tag{4}$$

The third column of the matrix representation of $\nabla\boldsymbol{\varphi}$ is empty because it is assumed that the membrane is a two-dimensional body. In order to introduce the contraction of the membrane thickness, stretch λ_Z along Z direction is introduced. Thus, the deformation gradient is defined as

$$[\mathbf{F}] = \begin{bmatrix} \rho_0\dfrac{\partial\alpha}{\partial R}\cos\alpha & 0 & \lambda_Z\sin\alpha \\ 0 & \dfrac{\rho_0\sin\alpha}{R} & 0 \\ -\rho_0\dfrac{\partial\alpha}{\partial R}\sin\alpha & 0 & \lambda_Z\cos\alpha \end{bmatrix}. \tag{5}$$

In this way we take into account that thickness H of the undeformed membrane transforms into $H' = \lambda_Z H$ in deformed configuration. The polar decomposition of the deformation gradient, $\mathbf{F} = \mathbf{RU}$, allows us to obtain the following rotation tensor $\mathbf{R}$ and pure deformation tensor $\mathbf{U}$:

$$[\mathbf{R}] = \begin{bmatrix} \cos\alpha & 0 & \sin\alpha \\ 0 & 1 & 0 \\ -\sin\alpha & 0 & \cos\alpha \end{bmatrix}, \qquad [\mathbf{U}] = \begin{bmatrix} \lambda_R & 0 & 0 \\ 0 & \lambda_\Theta & 0 \\ 0 & 0 & \lambda_Z \end{bmatrix}, \tag{6}$$

where

$$\lambda_R = \rho_0\frac{\partial\alpha}{\partial R} = \frac{2\alpha_0\rho_0}{L}, \qquad \lambda_\Theta = \frac{\rho_0\sin\alpha}{R}. \tag{7}$$

The fact that radial stretch λ_R is constant is a consequence of assuming that the membrane deforms into a spherical cap. Note that tensor $\mathbf{U}$ is diagonal because reference system (R,Θ,Z) is principal. The diagonal components of $\mathbf{U}$ are the principal stretches λ_R, λ_Θ and λ_Z. The right Cauchy-Green deformation tensor

$\mathbf{C} = \mathbf{F}^T\mathbf{F}$ reads

$$[\mathbf{C}] = \begin{bmatrix} \lambda_R^2 & 0 & 0 \\ 0 & \lambda_\Theta^2 & 0 \\ 0 & 0 & \lambda_Z^2 \end{bmatrix}, \tag{8}$$

with λ_R and λ_Θ given by Eq. (7).

Under the assumptions of frame-indifference and isotropy, the stored energy function ω of the material depends only on the principal invariants $\imath_j$ $(j = 1, 2, 3)$ of the right Cauchy-Green deformation tensor, defined as

$$\begin{aligned} \imath_1 &= \|\mathbf{F}\|^2 = \lambda_R^2 + \lambda_\Theta^2 + \lambda_Z^2, \\ \imath_2 &= \|\mathbf{F}^*\|^2 = \lambda_R^2\lambda_\Theta^2 + \lambda_R^2\lambda_Z^2 + \lambda_\Theta^2\lambda_Z^2, \\ \imath_3 &= (\det\mathbf{F})^2 = \lambda_R^2\lambda_\Theta^2\lambda_Z^2, \end{aligned} \tag{9}$$

where $\|\mathbf{F}\| = \mathrm{tr}\left(\mathbf{F}^T\mathbf{F}\right)^{1/2}$ and $\mathbf{F}^* = (\det\mathbf{F})\,\mathbf{F}^{-T}$ denotes the cofactor of the deformation gradient. The first Piola-Kirchhoff stress tensor is expressed by the constitutive equation

$$\mathbf{T}_R(\mathbf{F}) = \frac{\partial\omega}{\partial\mathbf{F}} = 2\left[\left(\frac{\partial\omega}{\partial\imath_1} + \imath_1\frac{\partial\omega}{\partial\imath_2}\right)\mathbf{F} - \frac{\partial\omega}{\partial\imath_2}\mathbf{R}\mathbf{U}^3 + \imath_3\frac{\partial\omega}{\partial\imath_3}\mathbf{R}\mathbf{U}^{-1}\right]. \tag{10}$$

This equation can be rewritten as

$$\mathbf{T}_R = \mathbf{R}\mathbf{S}, \tag{11}$$

where diagonal tensor $\mathbf{S}$ is the Biot stress tensor and is defined as

$$[\mathbf{S}] = \begin{bmatrix} S_R & 0 & 0 \\ 0 & S_\Theta & 0 \\ 0 & 0 & S_Z \end{bmatrix}, \tag{12}$$

with

$$S_J = 2\left[\left(\frac{\partial\omega}{\partial\imath_1} + \imath_1\frac{\partial\omega}{\partial\imath_2}\right)\lambda_J - \frac{\partial\omega}{\partial\imath_2}\lambda_J^3 + \imath_3\frac{\partial\omega}{\partial\imath_3}\lambda_J^{-1}\right], \quad \text{for } J = R, \Theta, Z. \tag{13}$$

The material behavior is defined by the compressible Mooney-Rivlin constitutive law [51, 52]

$$\omega(\imath_1, \imath_2, \imath_3) = a(\imath_1 - 3) + b(\imath_2 - 3) + c(\imath_3 - 1) - (a + 2b + c)\ln\imath_3, \tag{14}$$

where parameters a, b and c are positive scalars. Note that ω vanishes in the undeformed configuration, where $\lambda_R = \lambda_\Theta = \lambda_Z = 1$. Substituting Eq. (14) into Eq. (13), the components of tensor $\mathbf{S}$ become

$$\begin{aligned} S_R &= 2\lambda_R\left[a - \frac{a + 2b + c}{\lambda_R^2} + \lambda_\Theta^2\left(b + c\lambda_Z^2\right) + b\lambda_Z^2\right], \\ S_\Theta &= 2\lambda_\Theta\left[a - \frac{a + 2b + c}{\lambda_\Theta^2} + \lambda_Z^2\left(b + c\lambda_R^2\right) + b\lambda_R^2\right], \\ S_Z &= 2\lambda_Z\left[a - \frac{a + 2b + c}{\lambda_Z^2} + \lambda_\Theta^2\left(b + c\lambda_R^2\right) + b\lambda_R^2\right]. \end{aligned} \tag{15}$$

In the undeformed configuration $S_J = 0$ $(J = R, \Theta, Z)$, therefore the undeformed membrane is stress-free.

The membrane can only undergo a plane stress state and therefore condition $S_Z = 0$ must be fulfilled. This condition, using Eq. (15), allows us to derive the following relation between the principal stretches:

$$\lambda_Z = \sqrt{\frac{a + 2b + c}{a + \lambda_\Theta^2\left(b + c\lambda_R^2\right) + b\lambda_R^2}}. \tag{16}$$

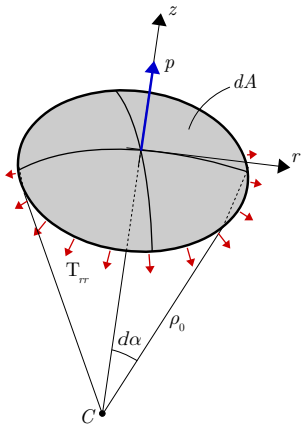

Figure 2: Local equilibrium in z direction written in the neighborhood of the central point of the circular membrane subjected to inflation. The applied pressure p is balanced by the radial stress component T_{rr}.

The above relation is valid for compressible hyperelastic materials and reduces to $\lambda_Z = 1/(\lambda_R \lambda_\Theta)$ when $c \to \infty$, which implies that $\det \mathbf{F} = 1$. This limit case corresponds to a solid that undergoes only isochoric deformations, namely it is incompressible. Hence, Eq. (16) gives λ_Z in the general case of circular membrane composed of a compressible material, while incompressibility is achieved when parameter c goes to infinity.

The Cauchy stress tensor is defined as $\tilde{\mathbf{T}} = (\det \mathbf{F})^{-1} \mathbf{T}_\mathbf{R} \mathbf{F}^T$ [53]. The principal directions (r, θ, z) for the Cauchy stress tensor are identified by applying the rotation given by tensor $\mathbf{R}$ to the material reference system (R, Θ, Z). Therefore, the diagonal form of the Cauchy stress tensor in the principal reference system is $\mathbf{T} = (\det \mathbf{F})^{-1} \mathbf{R}^T \mathbf{T}_\mathbf{R} \mathbf{F}^T \mathbf{R}$, which gives the following result:

$$
\begin{aligned}
\mathrm{T}_{rr} &= \frac{2}{\lambda_R \lambda_\Theta \lambda_Z} \left[a\left(\lambda_R^2 - 1\right) + b\left(\lambda_R^2 \lambda_Z^2 - 2\right) + \lambda_R^2 \lambda_\Theta^2 \left(b + c\lambda_Z^2\right) - c \right], \\
\mathrm{T}_{\theta\theta} &= \frac{2}{\lambda_R \lambda_\Theta \lambda_Z} \left[a\left(\lambda_\Theta^2 - 1\right) + b\left(\lambda_R^2 \lambda_\Theta^2 - 2\right) + \lambda_\Theta^2 \lambda_Z^2 \left(b + c\lambda_R^2\right) - c \right], \\
\mathrm{T}_{zz} &= \frac{2}{\lambda_R \lambda_\Theta \lambda_Z} \left[a\left(\lambda_Z^2 - 1\right) + b\left(\lambda_R^2 \lambda_Z^2 - 2\right) + \lambda_\Theta^2 \lambda_Z^2 \left(b + c\lambda_R^2\right) - c \right], \\
\mathrm{T}_{ij} &= \mathrm{T}_{ji} = 0,
\end{aligned}
\tag{17}
$$

where $i = r, \theta, z$ and $j = r, \theta, z$, with $i \neq j$. Substitution of Eq. (16) into Eq. (17) gives $\mathrm{T}_{zz} = 0$. This result is consistent with the fact that the membrane is in a state of plane stress.

After having derived the stress components, the equilibrium equations can be written. Since we adopted a semi-inverse method by setting a priori the kinematics of deformation, the local equilibrium equations can not be satisfied in every internal point of the membrane. However, an analytical solution can still be derived by solving the local equilibrium only in the neighborhood of the most representative point of the inflated membrane, namely the central point. To do this, we solve the equilibrium equation in z direction only for the case of $R \to 0$. Fig. 2 shows the external force generated by pressure p acting on area $dA = \pi \rho_0^2 d\alpha^2$. This force is balanced by the projection of the radial stress component T_{rr} along z direction, which acts on area $2\pi \rho_0 d\alpha H'$. With the approximation $\sin d\alpha \cong d\alpha$, the local equilibrium for $R \to 0$ reads

$$
p\left(\pi \rho_0^2 d\alpha^2\right) = d\alpha \left(2\pi \rho_0 d\alpha H'\right) \mathrm{T}_{rr}\big|_{R \to 0}, \tag{18}
$$

from which we derive the following expression for the applied pressure:

$$
p = \frac{2\left(\mathrm{T}_{rr} H'\right)\big|_{R \to 0}}{\rho_0}, \tag{19}
$$

with $H' = \lambda_Z H$ and λ_Z given by Eq. (16).

Principal stress component T_{rr} for the case of $R \to 0$ reads

$$\mathrm{T}_{rr}\big|_{R\to 0} = \frac{2\sin^2\alpha_0\left(\alpha_0^2\csc^2\alpha_0 - 1\right)\left(a + b\alpha_0^2\csc^2\alpha_0\right)\left[a + 2b + \alpha_0^2\csc^2\alpha_0(2b+c) + c\left(1+\alpha_0^4\csc^4\alpha_0\right)\right]}{\alpha_0^2\sqrt{(a+2b+c)\left(a+2b\alpha_0^2\csc^2\alpha_0 + c\alpha_0^4\csc^4\alpha_0\right)}}. \quad (20)$$

Transversal stretch λ_Z assumes the following form with $R \to 0$:

$$\lambda_Z\big|_{R\to 0} = \sqrt{\frac{a+2b+c}{a+2b\alpha_0^2\csc^2\alpha_0 + c\alpha_0^4\csc^4\alpha_0}}. \quad (21)$$

It is now convenient to introduce the normalized external pressure as $\bar{p} = pL/(2aH)$. The expression that links $\bar{p}$ to the kinematic parameter α_0 is finally derived by substituting Eqs. (20) and (21) into Eq. (19), obtaining

$$\bar{p} = \frac{4\sin^3\alpha_0\left(\alpha_0^2\csc^2\alpha_0 - 1\right)\left(a + b\alpha_0^2\csc^2\alpha_0\right)\left[a + 2b + \alpha_0^2\csc^2\alpha_0(2b+c) + c\left(1+\alpha_0^4\csc^4\alpha_0\right)\right]}{a\alpha_0^2\left(a+2b\alpha_0^2\csc^2\alpha_0 + c\alpha_0^4\csc^4\alpha_0\right)}. \quad (22)$$

The kinematics is governed by parameter α_0 (see Fig. 1(c)), which is related to displacement δ of the central node of the membrane through relation $\alpha_0 = 2\tan^{-1}\bar{\delta}$, with $\bar{\delta} = 2\delta/L$ indicating the normalized deflection. The expression of pressure $\bar{p}$ given by Eq. (22) can be thus written directly as a function of deflection $\bar{\delta}$. This provides the equilibrium path of the inflated membrane in terms of pressure-displacement curve. The expression of the pressure for incompressible materials is derived by computing the limit when c goes to infinity, which gives

$$\bar{p}\big|_{c\to\infty} = \frac{4\sin^7\alpha_0}{\alpha_0^6}\left(1+\beta\alpha_0^2\csc^2\alpha_0\right)\left(\alpha_0^6\csc^6\alpha_0 - 1\right), \quad (23)$$

where $\beta = b/a$. Note that in this case the membrane response in terms of normalized pressure-displacement curve is function solely of material parameter β.

The formulation presented above was developed in the context of nonlinear elasticity. The linearized theory is derived by introducing the hypothesis that both displacements and displacement gradients are small [54]. The mathematical developments are reported in Appendix A. The following expressions for the elastic constants of linear elasticity are obtained:

$$E = \frac{4(a+b)(a+4b+3c)}{a+3b+2c}, \qquad \nu = \frac{b+c}{a+3b+2c}. \quad (24)$$

Both Young's modulus E and Poisson's ratio ν of Eq. (24) correspond to those reported in [55] and [56]. In these two works, the authors analyzed respectively the finite bending of hyperelastic solids and the equilibrium of the von Mises truss in finite elasticity. In both works, a compressible Mooney-Rivlin material was adopted and the linearization of the theory allowed to derive the expressions of E and ν, which provide a link between the Mooney-Rivlin parameters and the elastic constants of linear elasticity. It is interesting to observe that, although the problems addressed by the authors involve different stress states, the expressions derived from the linearization correspond.

3. Extension of the analytical solution

In the proposed analytical model, the kinematics of deformation is described under the simplifying hypothesis that the membrane transforms into a spherical cap, which means that the deformed shape has constant curvature. Several authors studied the inflation of circular hyperelastic membranes under the general hypothesis of variable curvature [2, 29, 30]. They adopted an incompressible Mooney-Rivlin law for the material and derived the local equilibrium equations, which are expressed as a system of differential

equations. However, a closed-form solution to this system can not be derived and thus the authors proposed numerical solutions.

Since the kinematics of our model is approximated, the obtained solution is not exact. Hence, in this section, we adjust the formulation by introducing an additional polynomial function in the pressure-deflection relation expressed by Eq. (22). The polynomial is calibrated by using reference solutions from numerical simulations. In particular, we consider the numerical procedure proposed by Yang and Feng [29], which will be summarized in the following. We derive the numerical solutions for a wide range of values of material parameter β. The range of β considered covers the constitutive response of all rubber materials used in technological applications. Such solutions are then used to adjust Eq. (22). As a result, we derive an accurate adjusted pressure-deflection relation that can be applied to all rubber materials described by the Mooney-Rivlin model.

3.1. Numerical solution

In our model we assumed a certain kinematics by defining the displacement field of Eq. (1), from which we derived the deformation vector and the deformation gradient expressed by Eqs. (3) and (5), respectively. However, as previously pointed out, our inverse approach allows us to derive an analytical solution for the equilibrium that is not exact. Instead, an exact solution of the equilibrium problem can be derived only without specifying a certain displacement field. In this case, the principal stretches read

$$\begin{aligned} \lambda_R &= \sqrt{{\varphi'_R}^2 + {\varphi'_Z}^2}, \\ \lambda_\Theta &= \frac{\varphi_R}{R}, \end{aligned} \tag{25}$$

where the dependence of the quantities with radial coordinate R is omitted for the sake of simplicity. Since we are dealing with incompressible materials, the transversal stretch is computed as $\lambda_Z = R/\left(\varphi_R \sqrt{{\varphi'_R}^2 + {\varphi'_Z}^2}\right)$.

The equilibrium equations in radial and normal directions read

$$\begin{aligned} \frac{dN_{rr}}{d\varphi_R} + \frac{1}{\varphi_R}(N_{rr} - N_{\theta\theta}) &= 0, \\ K_{rr}N_{rr} + K_{\theta\theta}N_{\theta\theta} &= p, \end{aligned} \tag{26}$$

where K_{rr} and $K_{\theta\theta}$ are the principal curvatures in radial and circumferential directions respectively, while N_{rr} and $N_{\theta\theta}$ are the principal stress resultants with dimension of force per unit length. For incompressible Mooney-Rivlin materials, the principal stress resultants read

$$\begin{aligned} N_{rr} &= 2aH\left(1+\beta\lambda_\Theta^2\right)\left(\frac{\lambda_R}{\lambda_\Theta} - \frac{1}{\lambda_R^3\lambda_\Theta^3}\right), \\ N_{\theta\theta} &= 2aH\left(1+\beta\lambda_R^2\right)\left(\frac{\lambda_\Theta}{\lambda_R} - \frac{1}{\lambda_R^3\lambda_\Theta^3}\right), \end{aligned} \tag{27}$$

with $\beta = b/a$.

The principal curvatures are written as

$$\begin{aligned} K_{rr} &= \frac{\lambda'_R w - \lambda_R w'}{\lambda_R^2\sqrt{\lambda_R^2 - w^2}}, \\ K_{\theta\theta} &= \frac{\sqrt{\lambda_R^2 - w^2}}{\lambda_R\lambda_\Theta R}, \end{aligned} \tag{28}$$

where $w = \varphi'_R$. Substitution of Eqs. (27) and (28) into Eq. (26) gives the following system of equilibrium

equations:

$$\begin{aligned}
\lambda_R' &= \frac{\lambda_R\left[3\lambda_\Theta+\lambda_\Theta^3\left(\beta-\lambda_R^4\right)+\lambda_\Theta^4\lambda_R^2 w\left(1-\beta\lambda_R^2\right)+\beta\lambda_\Theta^5\lambda_R^4-w\left(\beta\lambda_R^2+3\right)\right]}{R\lambda_\Theta\left(\beta\lambda_\Theta^2+1\right)\left(\lambda_\Theta^2\lambda_R^4+3\right)},\\
\lambda_\Theta' &= \frac{w-\lambda_\Theta}{R},\\
w' &= \frac{w\lambda_R'}{\lambda_R}-\frac{\psi\lambda_\Theta^3\lambda_R^4\sqrt{\lambda_R^2-w^2}}{2R\left(\beta\lambda_\Theta^2+1\right)\left(\lambda_\Theta^2\lambda_R^4-1\right)}+\frac{\left(\beta\lambda_R^2+1\right)\left(\lambda_\Theta^4\lambda_R^2-1\right)\left(\lambda_R^2-w^2\right)}{R\lambda_\Theta\left(\beta\lambda_\Theta^2+1\right)\left(\lambda_\Theta^2\lambda_R^4-1\right)},
\end{aligned} \tag{29}$$

with $\psi = pR/aH$. Eq. (29) describes a boundary value problem and the boundary conditions are as follows. At the pole, principal stretches λ_R and λ_Θ are equal by symmetry and $\varphi_Z' = 0$. Thus, we have

$$\lambda_R = \lambda_\Theta = w = \lambda_0 \quad \text{at} \quad R = 0, \tag{30}$$

with $\lambda_0 > 1$. The membrane is fixed at the outer boundary, namely

$$\lambda_\Theta = 1 \quad \text{at} \quad R = L/2. \tag{31}$$

We are thus dealing with a two-point boundary value problem (TPBVP).

We can outline a simplified procedure for the numerical solution of Eq. (29) by observing that this system of equations remains unchanged if a generic scaling factor γ is multiplied to R. The numerical procedure is structured as follows:

1. set λ_0 to a desired value;
2. guess a value p_0 for pressure p;
3. solve Eq. (29) using the Runge-Kutta method, solving for increasing values of R until λ_Θ reaches unity;
4. the value R_0 corresponding to $\lambda_\Theta = 1$ will generally be different from $L/2$, since the guessed value p_0 for the pressure is not likely to be the correct one. However, we can now take advantage of the invariance property of Eq. (29). We choose a scaling factor γ such that

$$\gamma = \frac{L}{2R_0} \tag{32}$$

and

$$\bar{p} = \frac{p_0 R_0}{aH} = \frac{p_0 L}{2\gamma aH}. \tag{33}$$

Dividing the guessed value p_0 by the scaling factor γ we obtain the exact value of pressure that satisfies the equilibrium equations and the boundary conditions;
5. solve again the system with the correct value of pressure to obtain the stretches profiles. The deformed shape of the membrane is finally derived by computing φ_R and φ_Z from Eq. (25).

The governing equations depend on the Mooney-Rivlin parameters only through ratio β. Once fixed this parameter, variations of a cause only a scaling in the value of pressure. For this reason, it is straightforward to study the influence of the constitutive parameters on the solution of the problem. We defined a set of values for β ranging from 0 to 1, which is the typical range that can be found in the literature for real rubber materials [57–60]. All the rubbers employed in technological applications are characterized by a value of β included in such range and therefore the numerical simulations cover all the possible material behaviors. Overall, we considered 70 values for β. From value 0.04 to value 1 parameter β varies with a step of 0.02. The step decreases to 0.002 in the range 0–0.04, because in this range the transition between softening to hardening behaviour takes place and small variations of β are more significant. For each value of β, we obtained the corresponding solution of Eq. (29) by following the procedure described above.

The numerical integration of the differential equations was performed using function *ode23* in software MATLAB R2017a. For each value of β, we limited the analysis to a maximum stretch that did not exceed 7

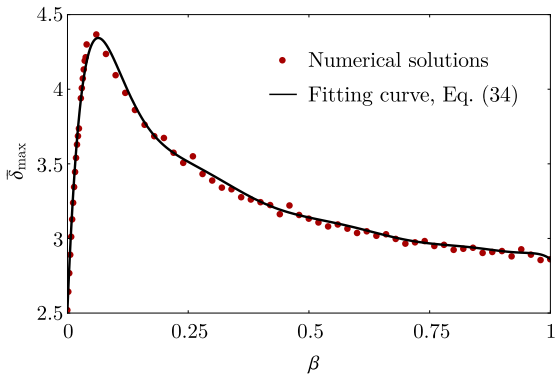

Figure 3: Values of normalized maximum deflection $\bar{\delta}_{\max} = 2\delta_{\max}/L$ obtained from the numerical solutions with variations of material parameter β (red dots) and fitting curve (continuous line), expressed by Eq. (34). The maximum deflection $\bar{\delta}_{\max}$ refers to the deflection of the central node, normalized over the radius, at which a radial stretch equal to 7 is reached somewhere in the membrane.

Table 1: Coefficients of the polynomial regression for $\bar{\delta}_{\max}$ that fits the values of maximum displacement obtained from the numerical solutions of the TPBVP.

c_0	c_1	c_2	c_3	c_4	c_5	c_6
c_7	c_8	c_9	c_{10}	c_{11}	c_{12}	
2.53024	74.3304	-973.79	3790.21	15676.8	-220381	1.02655×10^6
-2.72527×10^6	4.56501×10^6	-4.91994×10^6	3.31681×10^6	-1.27474×10^6	213391	

at any point of the membrane. This choice is consistent with physical evidence, since most rubbers subjected to uniaxial tensile test reach failure for stretches lower than 7 [61]. In the following, we indicate with $\bar{\delta}_{\max}$ the normalized vertical displacement at the pole that produces a radial stretch equal to 7 somewhere in the membrane. Note that the circumferential stretch λ_Θ always decreases moving from the pole to the outer boundary, due to the boundary condition $\lambda_\Theta(L/2) = 1$. Instead, the radial stretch λ_R increases or decreases depending on the constitutive parameters and on the magnitude of deformation. Therefore, λ_R does not always assume its maximum value at the central node of the membrane.

The values of $\bar{\delta}_{\max}$ obtained from the numerical simulations are displayed in Fig. 3, in function of β. As expected, different values of β correspond to different values of displacement $\bar{\delta}_{\max}$ of the central node at which a radial stretch equal to 7 is reached somewhere in the membrane. A regression law for $\bar{\delta}_{\max}$ as a function of β was estimated by using the *NonlinearModelFit* function of software Wolfram Mathematica. The following polynomial regression was derived:

$$\bar{\delta}_{\max}(\beta) = \sum_{i=0}^{12} c_i \beta^i, \tag{34}$$

with coefficients c_i, $i = 0, ..., 12$, listed in Tab. 1. The regression is displayed in Fig. 3, showing that it provides an accurate fit for the discrete values of maximum displacement obtained from the numerical simulations.

3.2. Extension of the analytical model and fitting to the numerical solution

In the following, we use the numerical solutions to adjust and extend the expression of pressure $\bar{p}$ given in Eq. (23). We recall that the numerical procedure by Yang and Feng is valid for incompressible materials. This is why we initially consider Eq. (23) for incompressible materials, extending the formulation to compressible materials later.

We adjusted the analytical expression of pressure in order to fit the numerical solutions of the TPBVP. This was done by applying a polynomial function of $\phi = \bar{\delta}/\bar{\delta}_{\max}$ with coefficients that vary as functions of parameter β. The advantage of introducing variable ϕ is that it varies in the range $[0,1]$. The adjusted expression of pressure becomes

$$\bar{p}_g = \bar{p} \sum_{j=1}^{10} f_j(\beta)\, \phi^j, \tag{35}$$

with $\bar{p}$ expressed by Eq. (23) and $\delta_{\max}$ given by Eq. (34). Functions $f_j(\beta)$, $j = 1,...,10$, assume a certain value for each of the values of β considered in the numerical simulations. In particular, the values of f_j were estimated by using the *NonlinearModelFit* function of software Wolfram Mathematica. *NonlinearModelFit* uses a least-square approach to find the values of f_j that allow to obtain the best fit of function $\bar{p}_g$ to the corresponding curve $\bar{p}$-ϕ obtained from the numerical simulation. This was done for each of the values of β considered.

At this point, *NonlinearModelFit* was applied again to derive the best fitting functions for the discrete values of f_j obtained for each β. For this purpose, we defined fitting polynomials with the following form:

$$f_j(\beta) = \sum_{k=0}^{12} d_{jk} \beta^k. \tag{36}$$

The best fitting coefficients d_{jk}, with $j = 1,...,10$ and $k = 0,...,12$, are listed in Tab. 2. The final adjusted expression for the pressure as a function of the deflection of the membrane is

$$\bar{p}_g = \bar{p} \sum_{j=1}^{10} \phi^j \sum_{k=0}^{12} d_{jk} \beta^k, \tag{37}$$

with $\bar{p}$ given by Eq. (23) and $\bar{\delta}_{\max}$ given by Eq. (34).

As previously mentioned, the numerical solution of the TPBVP is obtained with the hypothesis of incompressibility and therefore Eq. (37) is valid for incompressible materials only. However, the extension to compressible materials is immediate and the reason is explained in the following. Firstly, we remark that the kinematics of the analytical model of Section 2 is not dependent on the hypothesis of incompressibility. Indeed, the only stretch affected by compressibility parameter c is the transversal stretch λ_Z. Since we are dealing with a two-dimensional membrane, the transversal contraction has limited influence also on the exact deformed configuration that satifies the local equilibrium equations. Hence, the exact deformed configuration from the numerical solution is almost invariant to variations of c. In light of the above, the polynomial applied to $\bar{p}$ to adjust the analytical model remains unchanged in the case of compressible materials. The only thing that changes in Eq. (37) is the expression of pressure $\bar{p}$, which is computed by using Eq. (22) for compressible materials, instead of using Eq. (23). In the next section we will further validate this consideration by showing results of the model for compressible materials and a comparison with the numerical solution by Yang and Feng [29] extended to compressible membranes.

As we renounced to provide exact expressions for the kinematics of deformation of the membrane, the principal stretches given by Eq. (7) should be corrected as well. In particular, we are interested in adjusting the expression of principal radial and circumferential stretches at the pole

$$\lambda_\Theta\big|_{R\to 0} = \lambda_R = \frac{\alpha_0}{\sin\alpha_0}, \tag{38}$$

where we remind that $\alpha_0 = 2\tan^{-1}\bar{\delta}$. The same procedure as the one outlined above was adopted to fit the analytical stretch to the numerical one. The adjusted analytical expression for the stretch at the pole is

$$\lambda_g = \frac{\alpha_0}{\sin\alpha_0}\left(1 + \sum_{i=1}^{2} \phi^i \sum_{j=0}^{12} q_{ij} \beta^j\right), \tag{39}$$

Table 2: Coefficients estimated to fit the adjusted analytical expression of pressure, Eq. (37), to the numerical solutions of the TPBVP.

	d_{j0}	d_{j1}	d_{j2}	d_{j3}	d_{j4}	d_{j5}	d_{j6}
	d_{j7}	d_{j8}	d_{j9}	d_{j10}	d_{j11}	d_{j12}	
$j=1$	25.1332	53.3332	132.472	-18829.3	236715	-1.45801×10^{6}	5.37185×10^{6}
	-1.27304×10^{7}	1.99199×10^{7}	-2.04908×10^{7}	1.33391×10^{7}	-4.98462×10^{6}	814886	
$j=2$	-290.11	-1159.72	8012.55	175203	-2.92817×10^{6}	1.96593×10^{7}	-7.54752×10^{7}
	1.8305×10^{8}	-2.90441×10^{8}	3.01306×10^{8}	-1.97119×10^{8}	7.38465×10^{7}	-1.20818×10^{7}	
$j=3$	1894.3	13452.8	-220882	886565	5.24651×10^{6}	-6.82219×10^{7}	3.17859×10^{8}
	-8.44645×10^{8}	1.4102×10^{9}	-1.50832×10^{9}	1.00536×10^{9}	-3.80837×10^{8}	6.26759×10^{7}	
$j=4$	-7648.76	-86636.6	1.88396×10^{6}	-1.65039×10^{7}	7.40258×10^{7}	-1.66528×10^{8}	8.082×10^{7}
	5.39116×10^{8}	-1.55416×10^{9}	2.0668×10^{9}	-1.5402×10^{9}	6.20283×10^{8}	-1.05449×10^{8}	
$j=5$	19981.7	324566	-7.93754×10^{6}	8.29624×10^{7}	-4.91869×10^{8}	1.84277×10^{9}	-4.61641×10^{9}
	7.96896×10^{9}	-9.5814×10^{9}	7.9484×10^{9}	-4.37466×10^{9}	1.44806×10^{9}	-2.1921×10^{8}	
$j=6$	-34385.5	-737460	1.91095×10^{7}	-2.15162×10^{8}	1.39346×10^{9}	-5.77438×10^{9}	1.61574×10^{10}
	-3.13189×10^{10}	4.22467×10^{10}	-3.89975×10^{10}	2.35157×10^{10}	-8.34902×10^{9}	1.32333×10^{9}	
$j=7$	38714.9	1.03306×10^{6}	-2.76782×10^{7}	3.24712×10^{8}	-2.19771×10^{9}	9.52026×10^{9}	-2.77897×10^{10}
	5.59689×10^{10}	-7.80211×10^{10}	7.39699×10^{10}	-4.55222×10^{10}	1.63957×10^{10}	-2.62216×10^{9}	
$j=8$	-27441.4	-872992	2.39186×10^{7}	-2.88309×10^{8}	2.00596×10^{9}	-8.92019×10^{9}	2.66575×10^{10}
	-5.47812×10^{10}	7.76369×10^{10}	-7.45642×10^{10}	4.63322×10^{10}	-1.68001×10^{10}	2.69831×10^{9}	
$j=9$	11109	408387	-1.13809×10^{7}	1.39983×10^{8}	-9.93532×10^{8}	4.49908×10^{9}	-1.36587×10^{10}
	2.84384×10^{10}	-4.0728×10^{10}	3.94334×10^{10}	-2.46497×10^{10}	8.97545×10^{9}	-1.44547×10^{9}	
$j=10$	-1958.21	-81261.5	2.2969×10^{6}	-2.87188×10^{7}	2.07056×10^{8}	-9.50763×10^{8}	2.92054×10^{9}
	-6.13925×10^{9}	8.85893×10^{9}	-8.62692×10^{9}	5.41561×10^{9}	-1.97784×10^{9}	3.1915×10^{8}	

Table 3: Coefficients estimated to fit the adjusted analytical expression of the stretch at the pole, Eq. (39), to the numerical solutions of the TPBVP.

	q_{i0}	q_{i1}	q_{i2}	q_{i3}	q_{i4}	q_{i5}	q_{i6}
	q_{i7}	q_{i8}	q_{i9}	q_{i10}	q_{i11}	q_{i12}	
$i=1$	0.31271	77.1064	-2373.13	32253.9	-247831	1.19008×10^{6}	-3.76433×10^{6}
	8.05107×10^{6}	-1.1713×10^{7}	1.14212×10^{7}	-7.14247×10^{6}	2.58875×10^{6}	-413420	
$i=2$	0.740711	-124.238	3257.57	-41512.8	307550	-1.44223×10^{6}	4.48639×10^{6}
	-9.4773×10^{6}	1.36569×10^{7}	-1.32161×10^{7}	8.21416×10^{6}	-2.96201×10^{6}	470999	

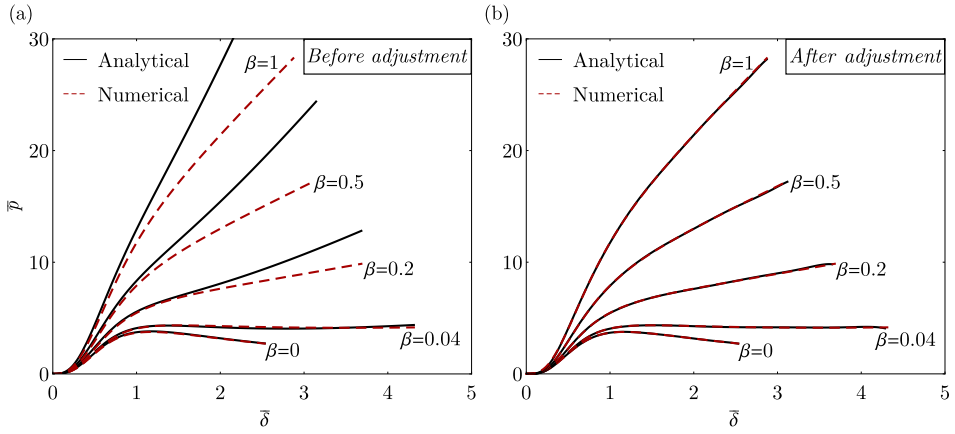

Figure 4: Normalized pressure $\bar{p}=pL/(2aH)$ vs. deflection $\bar{\delta}=2\delta/L$ for different values of β: (a) comparison between numerical solution and analytical pressure computed from Eq. (23); (b) comparison between numerical solution and adjusted analytical pressure computed from Eq. (37).

where coefficients q_{ij}, with $i=1,2$ and $j=0,...,12$, are listed in Tab. 3. The principal components S_R and S_Θ of the Piola-Kirchhoff stress tensor coincide at the central node. Their adjusted form was derived by imposing $\lambda_R=\lambda_\Theta=\lambda_g$ in Eq. (15). The following expression for the Piola stress at the pole was obtained:

$$\sigma_g=\frac{2\left(\lambda_g^2-1\right)\left(a+b\lambda_g^2\right)\left[a+2b+c+(2b+c)\lambda_g^2+c\lambda_g^4\right]}{\lambda_g\left(a+2b\lambda_g^2+c\lambda_g^4\right)}, \tag{40}$$

with λ_g given by Eq. (39).

Fig. 4(a) and 4(b) show respectively the analytical pressure-deflection curves before and after adjustment by fitting the numerical solutions. The plots are given for $\beta=0$, 0.04, 0.2, 0.5 and 1. The analytical pressure computed from Eq. (23) is accurate only for small values of β and relatively contained deformations, for which the assumption that the membrane deforms into a spherical cap is still appropriate. As β increases, significant discrepancies are observed at large deformations, as clearly visible in Fig. 4(a). Instead, the adjusted analytical pressure of Eq. (37) matches perfectly the numerical solution for every value of β, even for large deformations (Fig. 4(b)). It should be stressed that, although the analytical model was firstly developed under a simplifying assumption, it was necessary to proceed and derive a final accurate formulation. Having already an expression for $\bar{p}$ based on the physics of the problem made the fitting procedure much easier, which would have been otherwise very complex or even unfeasible.

On the other hand, as already pointed out, we renounced to provide exact expressions for the kinematics of the membrane. Theoretically, adjusting the analytical kinematics by fitting the deformed configuration of the numerical solution could be another possible approach. From the adjusted kinematics the analytical pressure

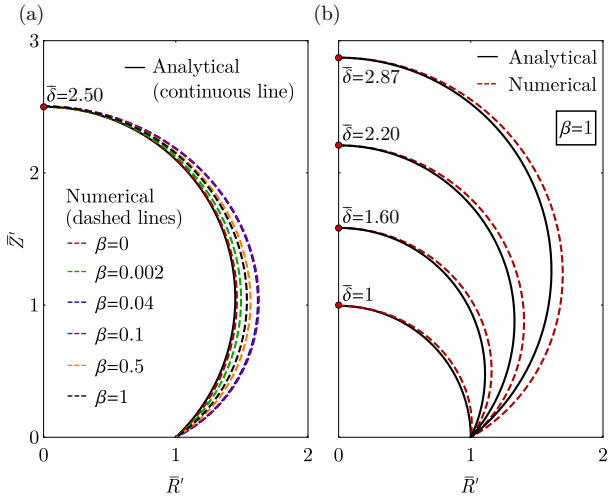

Figure 5: Normalized deformed shapes ($\bar{R}' = 2R'/L$ and $\bar{Z}' = 2Z'/L$) with (a) $\bar{\delta} = 2.5$ for different values of β and (b) $\beta = 1$ for different values of $\bar{\delta}$. The discrepancy between the spherical cap and the numerical deformed shape increases with the increasing of deflection and depends on the value of material parameter β.

can be obtained by substitution into the equilibrium equation Eq. (19). However, we found that very small discrepancies in the deformed configuration lead to considerable errors in the pressure-displacement curve, making this approach unpracticable. This is the reason why we renounced to adjust the kinematics of the membrane. In light of the above, a certain approximation on the deformed configuration must be accepted. Fig. 5(a) shows the deformed configuration at $\bar{\delta} = 2.5$ for different values of β. For $\beta = 0$ the numerical deformed shape is very close to a spherical cap, thus the discrepancy between analytical and numerical solution is minimum. For other values of β the error increases showing a trend similar to $\bar{\delta}_{\max}$, namely it has a peak around $\beta = 0.1$ and then it decreases. Fig. 5(b) compares the analytical and numerical solution for $\beta = 1$ at different values of $\bar{\delta}$. As expected, the discrepancy increases as the deformation increases. Note that for engineering applications the most important result for inflated membranes is the pressure-deflection curve, for which our extended analytical formulation gives a very accurate prediction. Instead, we accept a reasonable approximation on the deformed shape.

The sole kinematic quantity that we adjusted is the stretch at the pole, expressed by Eq. (38), from which the corresponding Piola stress was derived and given in Eq. (40). Fig. 6 shows the trend of stretch at the pole obtained from the numerical solution and the adjusted analytical stretch λ_g. Note that for large values of β (0.1, 0.5 and 1) the stretch at the pole does not reach maximum value 7 because it is reached elsewhere in the membrane.

4. Validation of the model

In this section we present a validation of the model proposed in this work. Firstly, the case of incompressible materials is considered. In particular, the proposed pressure-deflection relation, given by Eq. (37), is validated by showing a comparison with FE simulations and with the solutions proposed by other authors (Fichter [28], Yuan et al. [48] and Yang et al. [49]). Afterwards, we consider the case of compressible materials. We show the accuracy and effectiveness of our model even for this class of materials.

4.1. Finite element simulation

The FE simulations were carried out in software COMSOL Multiphysics version 6.0. The model was built using the 3D membrane interface of the structural mechanics module. In software COMSOL, membranes are plane stress elements in 3D that can deform both in the in-plane and out-of-plane directions. Differently

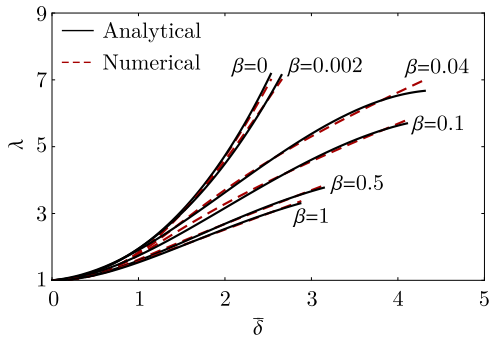

Figure 6: Representation of the stretch at the pole $\lambda_\Theta\big|_{R\to 0} = \lambda_R = \lambda$, expressed by Eq. (39). The curves are given for different values of β and are compared with the ones obtained from the numerical solutions of the TPBVP.

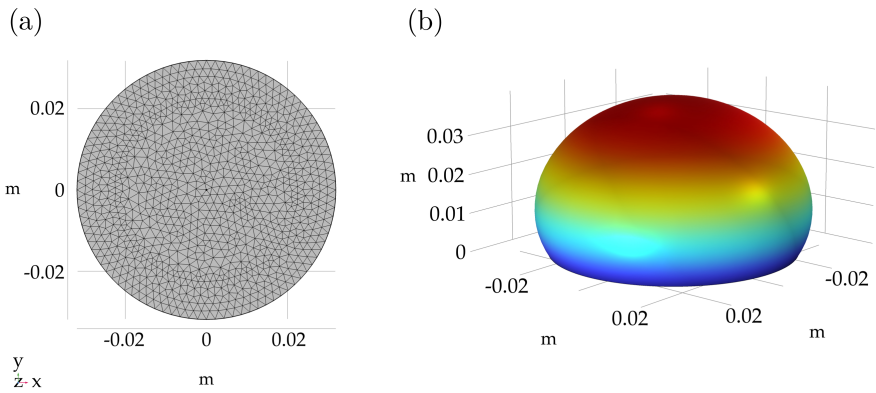

Figure 7: FE model of the inflated membrane created in COMSOL Multiphysics. (a) Meshed geometry of the membrane. (b) Deformed configuration after application of the uniform lateral pressure. The hyperelastic material was defined using the built-in two-parameter incompressible Mooney-Rivlin function. A stationary analysis was carried out and the pressure load increased linearly in a quasi-static manner.

from shell elements, membrane elements do not have bending stiffness. Since field variables do not change over time, a stationary study was selected.

A work plane was defined, in which we created a circle with diameter $L = 63.5$ mm. In the membrane settings we set the thickness $H = 1.57$ mm. Note that the numerical values of L and H have no influence, since the results will be reported in terms of normalized quantities. A fixed constraint was applied to the edges of the membrane, in this way the outer boundary was simply-supported. The hyperelastic material was defined using the built-in two-parameter incompressible Mooney-Rivlin energy function. Parameter a was set to 1 MPa, while parameter b varies in order to consider different cases of ratio β. In particular, the following simulations were carried out: $b = 0$ MPa, $b = 0.1$ MPa, $b = 0.25$ MPa, $b = 0.5$ MPa and $b = 1$ MPa.

The flat undeformed membrane has zero transverse stiffness and this generates a singularity. To avoid this, a tensile prestress was introduced through an external in-plane force of 10^{-4} N/m. The sole scope of the prestress was to allow the solver to find a solution. In fact, the prestress was negligible compared to the stress values acting on the membrane during the simulation. The membrane was discretized in a fine mesh composed of triangular elements with size around 0.6 mm (Fig. 7(a)). A pressure load was applied to the free face and increased linearly in a quasi-static manner, inflating the membrane. In particular, the increasing values of applied pressure were defined as a list in the auxiliary sweep of the stationary analysis. Geometric nonlinearities were taken into account because large deformations are involved.

The MUMPS solver was used for the stationary analysis. The simulation stopped at the last applied

value of pressure or when a stationary value was reached. In this case, for further increasing values of pressure, convergence was not found anymore and the analysis stopped. Fig. 7(b) shows the deformed configuration of the circular inflated membrane.

4.2. Other solutions from the literature

Only few analytical solutions can be found in the literature. A recent solution was proposed by Yuan et al. [48] for incompressible Mooney-Rivlin materials, assuming that the membrane deforms into a spherical cap. The expression of pressure as a function of deflection derived by Yuan et al. [48] is the following:

$$\bar{p}_{\text{Yuan}} = \frac{4\sin^7\alpha_0}{\alpha_0^6}\left(1+\beta\,\alpha_0^2\csc^2\alpha_0\right)\left(\alpha_0^6\csc^6\alpha_0-1\right), \tag{41}$$

with $\alpha_0 = 2\tan^{-1}\bar{\delta}$. Note that this solution corresponds to Eq. (23), which was obtained by computing the limit of our analytical solution for the case of incompressible materials. The correspondence of Eqs. (41) and (23) is not a surprise, because both formulations were obtained under the same assumption on the kinematics of deformation of the membrane.

Another analytical solution for pre-stretched inflated membranes was derived by Yang et al. [49] for the case of neo-Hookean materials. Since the membrane is pre-stretched, both radial and circumferential stretches are assumed to be very large. Therefore, as already made by Foster [62], the authors assumed that term $\lambda_R^{-3}\lambda_\Theta^{-3}$ is negligible with respect to λ_R/λ_Θ and λ_Θ/λ_R. Under this assumption, the solution proposed in [49] is

$$\bar{p}_{\text{Yang}} = \frac{8\bar{\delta}}{1+\bar{\delta}^2}. \tag{42}$$

It goes without saying that this solution is not accurate for relatively small deformations. However, it gives an accurate description of the inflation of the membrane when deformations become very large.

The last solution that we consider is the one proposed by Fichter [28]. In this case, the author assumed a linearly elastic constitutive law for the material. The equilibrium equations are

$$\begin{aligned} &N^2\left(\bar{R}^2\frac{d^2N}{d\bar{R}^2}+3\bar{R}\frac{dN}{d\bar{R}}\right)-\frac{1}{2}\bar{R}^3\frac{dN}{d\bar{R}}+\frac{1}{2}(3+\nu)\,\bar{R}^2N+\frac{1}{4}\frac{\bar{R}^2EH}{pL}=0,\\ &N\frac{d\bar{\delta}}{d\bar{R}}+\frac{1}{2}\bar{R}=0, \end{aligned} \tag{43}$$

where $\bar{R} = 2R/L$, E is the Young's modulus, ν is the Poisson's ratio and $N = 2N_{rr}/(pL)$, with N_{rr} indicating the radial stress resultant. The solution for both stress resultant and deflection is found in the form of a power series

$$\begin{aligned} N\left(\bar{R}\right) &= \sum_0^\infty n_{2m}\bar{R}^{2m},\\ \bar{\delta}\left(\bar{R}\right) &= \sum_0^\infty w_{2n}\left(1-\bar{R}^{2n+2}\right). \end{aligned} \tag{44}$$

The expressions of the first six coefficients n_i and w_i of the power series for N and $\bar{\delta}$ are reported in [28]. In the present work, in order to increase the accuracy of the solution, we consider the first twelve terms of both power series. The procedure for the determination of coefficients n_i and w_i is outlined in [28].

4.3. Results and comparison

The normalized pressure-deflection curve of Eq. (37) is compared with the FE simulation and the other solutions described above. Note that the solution by Fichter [28] involves the elastic constants E and ν. These two constants are computed using Eq. (24), after having set material parameters a and b. We remind that we are still dealing with incompressible materials, therefore $c \to \infty$.

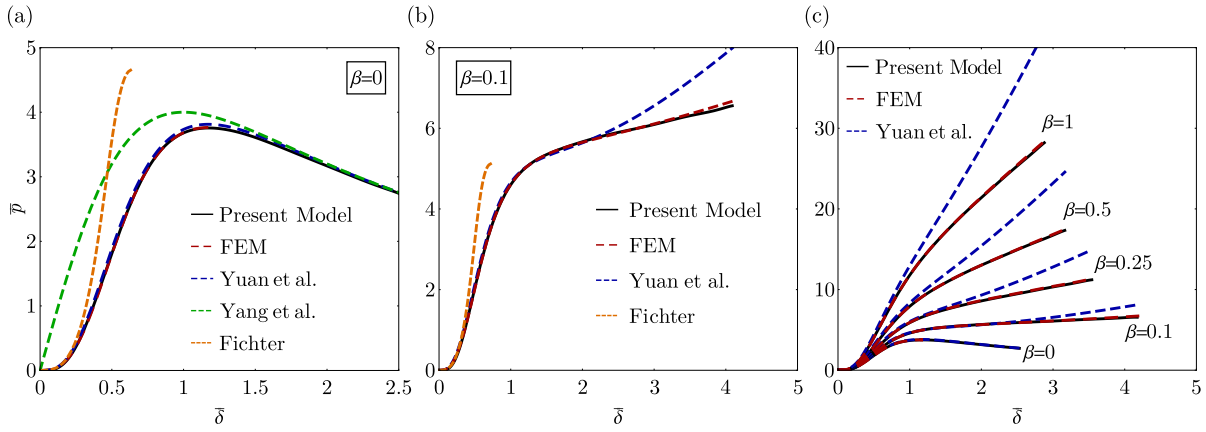

Figure 8: Comparison of pressure-deflection curves obtained with present analytical model (Eq. (37)), FE simulations and other solutions found in the literature: (a) Neo-Hookean material ($\beta = 0$); (b) Mooney-Rivlin material with $\beta = 0.1$; (c) variations of material parameter β.

Fig. 8(a) shows a comparison of the solutions in the case of neo-Hookean material ($\beta = 0$). We observe that the prediction of our analytical model agrees perfectly with the FE simulation. Note that the equilibrium path exhibits a softening branch after the maximum value of pressure. Since the FE analysis is carried out in force control, the FE model is not able to capture this softening branch. The solution by Yuan et al., expressed in Eq. (41), is also quite accurate. This because when $\beta = 0$ the hypothesis that the deformed shape follows a spherical cap is appropriate (see Fig. 5(a)). As expected, the solution by Yang et al. given in Eq. (42) is completely wrong for small deflections. Instead, when deformations become very large, this solution agrees well with both FEM and our analytical prediction. Finally, the solution by Fichter is accurate only until deflections around one third of the radius of the membrane. For larger deflections, this solution is much stiffer than the others. This happens because the material is linearly elastic, which is a suitable approximation only when deformations are small. Fichter's solution is not capable of capturing the nonlinearities in the material behavior.

Fig. 8(b) shows a comparison of the results for an incompressible Mooney-Rivlin material with $\beta = 0.1$. Again, there is a very good agreement between our model and the FE simulation. Differently from the case $\beta = 0$, the solution by Yuan et al. is not accurate. In particular, the larger the deflection is, the more the deformed shape deviates from a spherical cap. Consequently, the error in the prediction by Yuan et al. increases. The solution by Yang et al. is not reported because it is valid only for neo-Hookean materials.

The comparison of pressure-deflection curves for various values of β in the range 0 to 1 is given in Fig. 8(c). In particular, we compare the solutions obtained with our analytical model, the FE simulation and the formulation proposed by Yuan et al. For each value of β, the analytical model proposed in the present work gives a result that is in good agreement with the FE simulation. On the other hand, the solution by Yuan et al. can be considered accurate only for values of β that are very close to 0. This demonstrates that our adjusted model is capable of predicting the response of an inflated membrane composed of Mooney-Rivlin material. Instead, other analytical solutions based on simplifying assumptions may be accurate only for certain material properties or magnitude of deformation. For instance, the solution by Fichter is only reliable for small deformations, while the solution by Yang et al. only for very large deformations and neo-Hookean material.

4.4. Compressible materials

In the literature, solutions for the inflation of circular membranes in the context of large deformations can be found only for incompressible materials. In the present work, we provide a solution for the general case of compressible materials. As already mentioned, the extension of our proposed model to the class of compressible materials is straightforward. This because we are dealing with a two-dimensional membrane

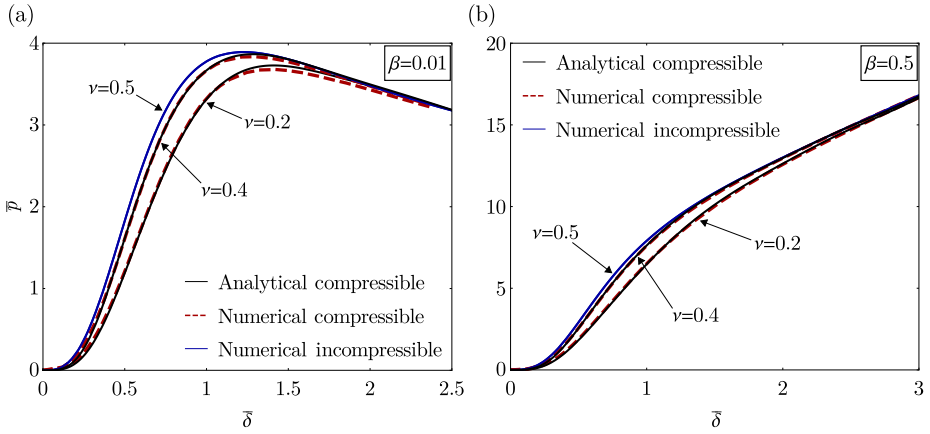

Figure 9: Pressure-deflection curves for compressible membranes: (a) $\eta = 0.326$ ($\nu = 0.2$), $\eta = 2.01$ ($\nu = 0.4$) and $\eta \to \infty$ ($\nu = 0.5$) in the case of $\beta = 0.01$; (b) $\eta = 0$ ($\nu = 0.2$), $\eta = 2.5$ ($\nu = 0.4$) and $\eta \to \infty$ ($\nu = 0.5$) in the case of $\beta = 0.5$. The analytical curve is obtained from Eq. (37), with $\bar{p}$ given by Eq. (22). The numerical solution is obtained as described in Appendix B. Variations of compressibility parameter ($\eta = c/a$) produce sensible differences in the pressure-deflection response.

and therefore the transversal contraction has a small influence on the shape of the deformed configuration. Hence, Eq. (37) maintains its effectiveness, provided that the expression of $\bar{p}$ is taken from Eq. (22) instead of Eq. (23). To prove this, in the following we show a comparison with a reference numerical solution.

To derive a reference solution, we extended the numerical solution by Yang and Feng to the class of compressible materials. To this aim, we replaced the Mooney-Rivlin constitutive law for incompressible materials, expressed by Eq. (27), with the Mooney-Rivlin law for compressible materials. The detailed derivation of the equilibrium equations for compressible materials and the numerical solution of the corresponding TPBVP can be found in Appendix B.

Fig. 9 shows a comparison of the numerical solution for compressible materials and the adjusted analytical solution proposed in this work. We remind that the analytical model (continuous black lines) for compressible materials is expressed by Eq. (37), in which $\bar{p}$ is given by Eq. (22). The red dashed lines represent the numerical solution extended to compressible materials while the continuous blue lines represent the numerical solution for incompressible materials ($\nu = 0.5$).

We focused on the two cases $\beta = 0.01$ and $\beta = 0.5$, in order to consider both softening and hardening behaviors. For each case, we selected two values of parameter $\eta = c/a$, such that Poisson's ratio ν equals 0.2 and 0.4. We recall that the Poisson's ratio is linked to the Mooney-Rivlin parameters through Eq. (24), which is rewritten as a function of only β and η as

$$\nu = \frac{\beta + \eta}{1 + 3\beta + 2\eta}. \tag{45}$$

From Fig. 9, we observe that the two curves derived from analytical and numerical models are in good agreement. This proves that the analytical model proposed in this work gives accurate predictions also in the most general case of compressible materials.

It is worth noting that, as expected, incompressible membranes are always stiffer than compressible ones. This is explained by the fact that incompressible solids can not undergo volume variations. In addition, from Fig. 9 we note that compressibility mainly affects the first part of the pressure curve and its impact is more significant for low values of β. In general, variations of η produce a sensible variation in the pressure-deflection curve. Therefore, it should be always checked that the hypothesis of incompressibility actually reflects the real behavior of the material considered. If not, the model proposed in the present work is a valid tool for the prediction of the inflation of compressible membranes.

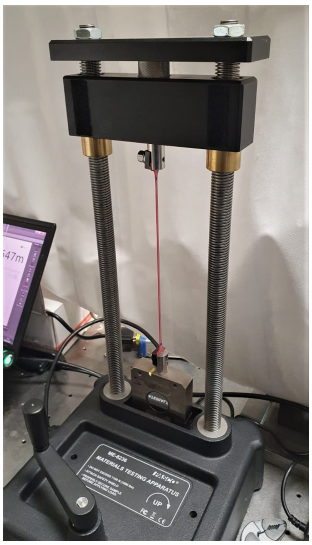

Figure 10: Set up of the uniaxial tensile test. The dog-bone specimen was fixed at the bottom and connected to the load bar at the top. A crank gear was used to raise the load bar and stretch the specimen. Force and displacement data were recorded. The tests were carried out on styrene butadiene rubber (SBR), latex and silicone.

5. Experimental characterization of rubber materials

We considered three kinds of rubber: styrene butadiene rubber (SBR), latex and silicone. Each rubber was available as a sheet. The thickness of the SBR and latex sheets was 1 mm, while that of the silicone sheet was 0.5 mm. Uniaxial tensile tests and bulge tests were carried out. The parameters of the Mooney-Rivlin law were estimated for each rubber in order to fit the experimental data.

In this section we firstly present the experimental tests. Then, we describe the calibration of parameters a, b and c of the Mooney-Rivlin constitutive law. Finally, we compare the experimental and analytical results to show that the proposed model reproduces well the experimental response.

5.1. Experimental tests

Three uniaxial tensile tests were carried out for each rubber. The dog-bone specimens had the same thickness of the rubber sheets, a width of 4 mm and an effective length of 40 mm. The tests were performed by using the materials testing apparatus ME-8236 produced by PASCO (Fig. 10). The machine has a built-in load cell (strain gauge transducer) capable of measuring up to 7100 newtons. An optical encoder module measures the displacement of the load bar. A crank gear raises or lowers the load bar on two translation screws. Force data from the load cell and displacement data from the encoder module were recorded, displayed and analyzed using the PASCO PASPORT Compatible Interface with the PASCO Data Collection Software. The sensor cable from the testing machine was connected to the PASPORT input port. Then, the USB link connected the PASCO Interface to a USB port on a laptop. Nominal stress and stretch were computed for each test.

After the uniaxial tensile tests, three bulge tests were carried out for each rubber. The setup of the tests is shown in Figs. 11(a) and 11(b). A steel plate with a circular hole in the center was supported by four pillars. The circular hole has diameter of 15 mm and the rubber membrane was placed above it. A striking plate was positioned on top to fix the membrane and a pressure was applied from above. As shown in Fig. 11(c), the deflection of central point of the membrane was monitored with a laser placed at the bottom of the system. Fig. 11(d) shows the deformation of the membrane during the test.

An aluminium tank was pressurized by a low-pressure compressor using an air compression gun equipped with a one-way valve. The pressure inside the tank was measured using the pressure transmitter TR2101100 produced by Trafag International. The gauge has a 0-10 bar measuring range and precision of 0.03 bar. The

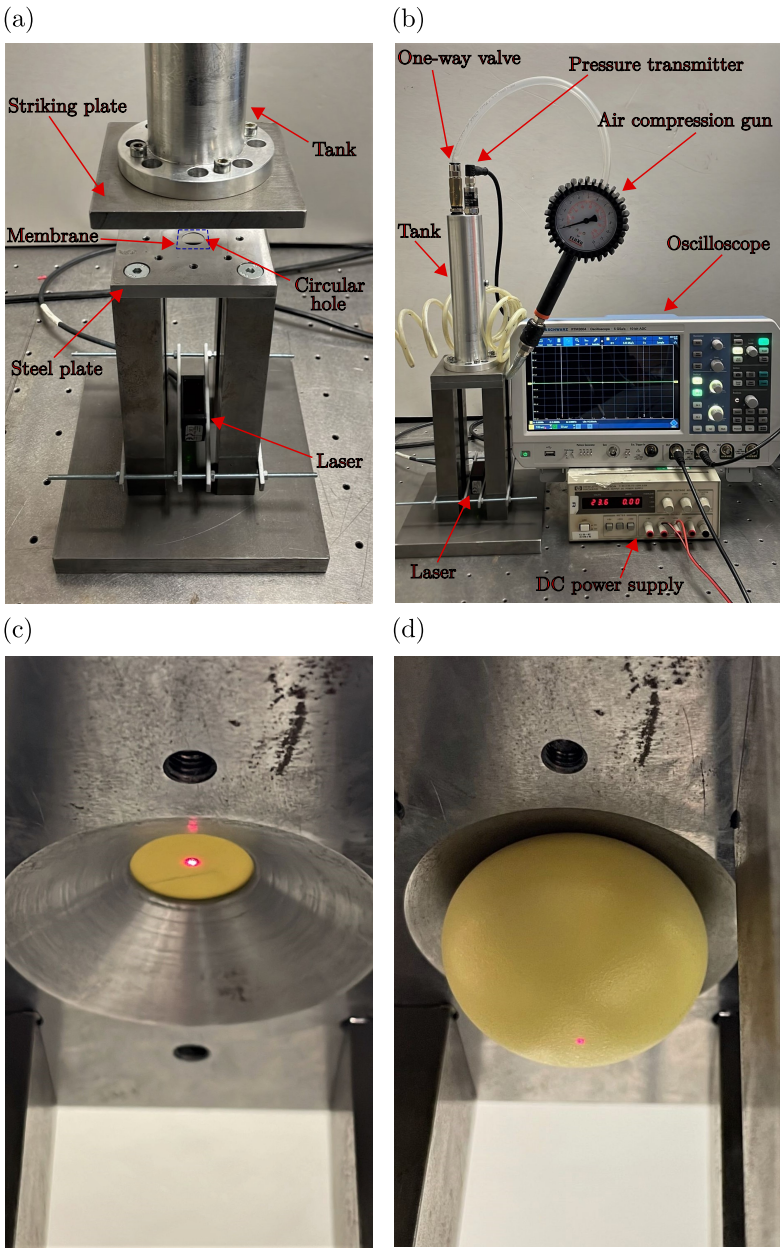

Figure 11: Bulge test on the circular rubber membrane. (a) The membrane was placed over a circular hole in a steel plate. An upper striking plate was used to fix the membrane. The pressure was applied from above into an aluminum tank and it was measured with a pressure transmitter, as shown in (b). The deflection of central point of the membrane was monitored with a laser placed at the bottom of the system. The tests were carried out on SBR, latex and silicone. Figures (c) and (d) show, respectively, the membrane in initial configuration and after inflation.

pressure gauge was powered by a 24 V DC power supply unit. The output current signal was converted into the corresponding value of pressure with a 4-20 mA current loop operation. A 270 Ω resistor was inserted into the current path and a Rohde & Schwarz RTM3004 oscilloscope measured the voltage drop across the resistor with a sampling rate of 3.33 MSa/s.

The deflection of the inflated membrane was measured using the OPTO1420 laser sensor produced by

Table 4: Mooney-Rivlin parameters calibrated by fitting experimental data from uniaxial and bulge tests.

	SBR	Latex	Silicone
a (MPa)	1.1	0.262	0.27
b (MPa)	0.1	0.012	0.03
β	0.091	0.046	0.111

Microepsilon. The sensor has a measuring range of 10-500 mm with a 0.01 mm precision. The deflection was also measured with a 4-20 mA current loop operation. The analogue voltage signals proportional to pressure and deflection were simultaneously acquired by the Rohde & Schwarz RTM3004 oscilloscope and exported as .csv files. The data files were then processed using MATLAB and the pressure-deflection curve was obtained.

5.2. Calibration of model parameters

The constitutive parameters of the Mooney-Rivlin material were initially calibrated by fitting the data from the uniaxial tensile tests for each rubber. The analytical model for compressible Mooney-Rivlin solids subjected to uniaxial tractions was developed by Lanzoni and Tarantino [63]. The expression of longitudinal Piola stress as a function of longitudinal stretch is reported in Eq. (50) of work [63], with damage parameter set to zero. We fitted the above equation to our data from uniaxial tensile tests for each rubber using the *NonlinearModelFit* function of software Wolfram Mathematica.

The calibration of parameters a, b and c was done for all three tests and for each rubber. Since there is not much variability in the experimental responses, the average values were taken as final reference values. For each rubber specimen, the calibration gave as a result a very high value of parameter c, which means that Poisson's ratio ν is close to 0.5. Therefore, we assumed that the rubbers analyzed are incompressible. This allowed us to calibrate only parameters a and b of the Mooney-Rivlin material, since $c \to \infty$. Note that we made this assumption to simplify the characterization of the material and show an application of the model proposed in this work. However, in a general case, incompressibility of the material should be checked with measurements of the lateral stretch during the uniaxial tensile test, as for instance was done in [64]. In such work, the authors analyzed a silicone rubber and discovered that, for this material, compressibility plays an important role and increases with the increasing of the elongation. In light of this, a comprehensive characterization of rubber materials should also consider experimental data of transversal stretch as a function of longitudinal stretch. Nevertheless, the scope of the present section is to give the approach for using the model proposed and show its benefits. This is why we adopted the hypothesis of incompressiblity, which may not be the most accurate approach.

After calibration on uniaxial tensile tests, the constitutive parameters were used to compute the analytical pressure-deflection curves by means of Eq. (37). The analytical and experimental results were compared for each of the circular rubber membranes tested. As expected, the best fitting parameters for the uniaxial tests did not represent the best choice also for the bulge tests. Therefore, parameters a and b were adjusted manually in order to obtain a final fit that represents the best compromise for both uniaxial and bulge tests. Such parameters for each rubber specimen are listed in Tab. 4. The corresponding analytical responses for uniaxial tensile tests are displayed in Fig. 12, along with the experimental data.

From Fig. 12 we observe that the Mooney-Rivlin constitutive law is very accurate for the SBR rubber. This because SBR breaks at a stretch around 2, which is relatively small. The analytical prediction is acceptable also for latex rubber. However, it is well know in the literature that the Mooney-Rivlin material model is not capable of describing strong hardening of polymers [58]. In fact, the calibrated analytical response for silicone is accurate only for stretches lower than 3. For larger stretches, silicone shows a very pronounced hardening and the material model is not capable of capturing such behavior. In light of this, the characterization of silicone requires a more refined constitutive law, such as the Ogden model [65] and the Yeoh model [66]. Nevertheless, for stretches less than 3 the analytical prediction is accurate and allows us to draw interesting conclusions and comparisons with the results of the bulge tests.

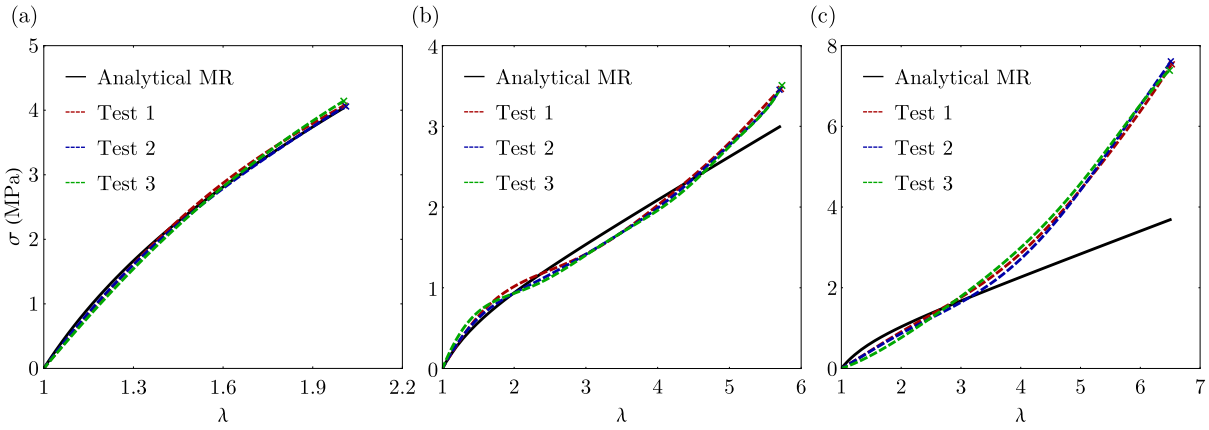

Figure 12: Piola stress σ vs. longitudinal stretch λ from uniaxial tensile tests and fitting with Mooney-Rivlin (MR) constitutive law for (a) SBR, (b) latex and (c) silicone. The analytical MR law used is reported in [63] and the constitutive parameters are listed in Tab. 4.

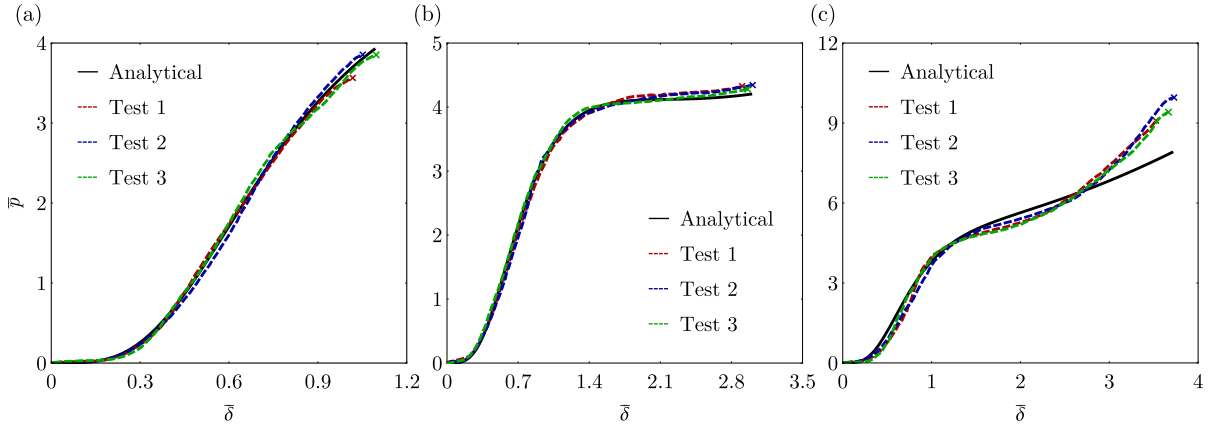

Figure 13: Pressure-deflection curves from bulge tests and comparison with analytical predictions for (a) SBR, (b) latex and (c) silicone. The analytical curves are obtained using Eq. (37) with the constitutive parameters listed in Tab. 4.

The analytical and experimental responses of the inflated circular membranes are shown in Fig. 13. Since the uniaxial response of SBR is accurately depicted by the Mooney-Rivlin law, also the result of the bulge test is in good agreement with the experimental data. Same goes for the latex rubber, with the exception of the final part of the curve with $\overline{\delta} > 2.5$. In accordance with the corresponding uniaxial response (Fig. 12(b)), latex rubber shows a slight hardening that is not captured by the Mooney-Rivlin law. This is the reason of the gap between analytical prediction and experimental curve in Fig. 13(b). The tests on silicone showed the same trend as the uniaxial tensile tests of Fig. 12(c). The analytical prediction of the inflation of the silicone membrane is accurate only until a deflection $\overline{\delta} \approx 2.5$, after which hardening takes place and the Mooney-Rivlin material is not suitable anymore.

It is important to stress that the characterization of polymers can not be done only on the basis of uniaxial tensile tests. As previously mentioned, the best fitting parameters derived from the uniaxial experiments were not accurate for the case of bulge test. Hence, the set of parameters was adjusted a posteriori. It was discovered that small variations of a and b cause sensible variations in the response of the membrane subjected to inflation. However, under such variations, the uniaxial response is almost the same. In light of the above, a reliable characterization of rubbers must take into account several stress states. To this regard, the pressure-deflection relation for the inflation of circular membranes proposed in this work is a useful and

straightforward tool.

6. Conclusions

An analytical formulation for the equilibrium problem of the inflation of circular flat membranes was presented. The theory was developed in finite elasticity and the material behavior was described by a compressible Mooney-Rivlin hyperelastic law. Under the assumption that the membrane deforms into a spherical cap, the equilibrium for $R \to 0$ was written and an expression of the pressure as a function of the deflection was derived.

The solution was affected by the simplifying hypothesis on the kinematics of deformation. Therefore, it was adjusted a posteriori by introducing a multiplicative polynomial function. The polynomial coefficients were determined by fitting the numerical solution provided by Yang and Feng [29] for the case of incompressible material. As a result, we derived an analytical formula describing the pressure-deflection relation for Mooney-Rivlin circular membranes as a function of material parameter β. The validation of the proposed analytical model was done by carrying out a FE simulation. The pressure-deflection curve provided by the FE analysis was in excellent agreement with the formula proposed.

A comparison with other solutions found in the literature proved the advantages of our model. The value of our approach was also confirmed, since the adjustment performed through the polynomial allowed to obtain excellent accuracy, preserving the advantage of having an analytical expression based on a simplified model. Being extremely accurate and easy-to-use, the analytical formula proposed in this work represents a novelty in the context of inflated membranes. It is a quick and reliable tool that can be used for several applications as well as the characterization of constitutive parameters for rubber materials.

As far as the authors know, all the other works in the literature dealing with finite inflation of hyperelastic membranes are based on the assumption of material incompressiblity. Our analytical model is instead applicable also to compressible materials. It was found that variations of parameter c cause significant changes in the pressure-deflection curve. This demonstrates the necessity to carefully check the hypothesis of incompressibility when dealing with real materials. This work fills a void in the literature by providing the expression of the pressure-deflection curve in case of compressible Mooney-Rivlin material.

Experimental uniaxial tensile tests an bulge tests were carried out on three kinds of rubber: SBR, latex and silicone. The analytical formula proposed in this work was applied for the characterization of the Mooney-Rivlin parameters. A good match between experimental and analytical behaviors was obtained for both SBR and latex rubbers. For silicone rubber significant errors were found after stretches greater than 3. This because at very large deformations silicone exhibits a pronounced hardening, which is not captured by the Mooney-Rivlin material model. The results showed that a comprehensive characterization of rubbers must take into account several stress states, not only uniaxial. To this end, the proposed pressure-deflection relation for the inflation of circular membranes is a useful and straightforward tool.

Forthcoming works will focus on the extension of the analytical model to pre-stretched membranes. More refined hyperelastic constitutive laws will be considered, so that rubber materials with strong hardening can be accurately modeled. To this regard, we may consider hyperelastic models such as the ones proposed by Ogden [65] and Yeoh [66].

Acknowledgements

This work was supported by the Italian Ministry of University and Research (MUR) through research grant PRIN 2020 No. 2020EBLPLS on “Opportunities and challenges of nanotechnology in advanced and green construction materials” and through project FISR 2019 “Eco Earth” (code 00245). Financial support by the National Group of Mathematical Physics (GNFM-INdAM) n.prot. U-UFMBAZ-2021-000085 is also acknowledged.

Appendix A. Linearized theory

The components of the right Cauchy-Green deformation tensor, expressed by Eq. (8), are developed in Taylor series as functions of α_0. The following expressions are obtained by truncating the series at the second order:

$$[\mathbf{C}] \cong \begin{bmatrix} \frac{1}{3}\left(\alpha_0^2+3\right) & 0 & 0 \\ 0 & \left(\frac{1}{3}-\frac{4R^2}{3L^2}\right)\alpha_0^2+1 & 0 \\ 0 & 0 & 1-\frac{2(b+c)\left(L^2-2R^2\right)\alpha_0^2}{3(a+2b+c)L^2} \end{bmatrix}. \tag{A.1}$$

The strain tensor of the linearized theory of elasticity is then computed as

$$[\mathbf{E}] = \frac{1}{2}[\mathbf{C}-\mathbf{I}] = \begin{bmatrix} \frac{\alpha_0^2}{6} & 0 & 0 \\ 0 & \frac{\left(L^2-4R^2\right)\alpha_0^2}{6L^2} & 0 \\ 0 & 0 & -\frac{(b+c)\left(L^2-2R^2\right)\alpha_0^2}{3(a+2b+c)L^2} \end{bmatrix}. \tag{A.2}$$

The linearization of stress tensor $\mathbf{S}$ provides

$$\begin{aligned} S_R &\cong \frac{2(a+b)\left[(a+4b+3c)L^2-4(b+c)R^2\right]\alpha_0^2}{3(a+2b+c)L^2}, \\ S_\Theta &\cong \frac{2(a+b)\left[(a+4b+3c)L^2-4(a+3b+2c)R^2\right]\alpha_0^2}{3(a+2b+c)L^2}, \\ S_Z &= 0. \end{aligned} \tag{A.3}$$

It can be easily verified that the linearized form of the Piola-Kirchhoff stress tensor $\mathbf{T_R}$ coincides with the linearized form of the Cauchy stress tensor $\mathbf{T}$.

The Navier's inverse relations in linear elasticity for the case of an inflated circular membrane read

$$\begin{aligned} \sigma_R &= \frac{E}{1-\nu^2}\left(\epsilon_R+\nu\epsilon_\Theta\right), \\ \sigma_\Theta &= \frac{E}{1-\nu^2}\left(\epsilon_\Theta+\nu\epsilon_R\right). \end{aligned} \tag{A.4}$$

A linear system of two equations is obtained by imposing the equivalence of σ_R and σ_Θ with the corresponding components S_R and S_Θ of the linearized stress tensor, expressed by Eq. (A.3). Strain components ϵ_R and ϵ_Θ are given respectively by E_{11} and E_{22} of Eq. (A.2). The system reads

$$\begin{aligned} \frac{4(a+b)\left[L^2(a+4b+3c)-4R^2(b+c)\right]}{a+2b+c} + \frac{E\left[L^2(\nu+1)-4\nu R^2\right]}{\nu^2-1} &= 0, \\ \frac{4(a+b)\left[L^2(a+4b+3c)-4R^2(a+3b+2c)\right]}{a+2b+c} + \frac{E\left[L^2(\nu+1)-4R^2\right]}{\nu^2-1} &= 0. \end{aligned} \tag{A.5}$$

The solution of this linear system gives the expressions of E and ν reported in Eq. (24). The strain component ϵ_Z in linear elasticity is expressed by

$$\epsilon_Z = -\frac{\nu}{E}\left(\sigma_R+\sigma_\Theta\right). \tag{A.6}$$

Using Eqs. (24) and (A.3) it can be easily verified that the expression of ϵ_Z corresponds to component E_{33} of the strain tensor in Eq. (A.2).

Appendix B. Numerical solution of the TPBVP for compressible Mooney-Rivlin materials

Firstly, the exact equilibrium equations for compressible Mooney-Rivlin materials are derived. We recall that, under the most general kinematics of deformation, principal stretches λ_R and λ_Θ are given by Eq. (25). Since we are dealing with compressible materials, transversal stretch λ_Z is expressed by Eq. (16) and the principal Cauchy stress components are given in Eq. (17). The stress resultants N_{rr} and $N_{\theta\theta}$, in radial and circumferential directions respectively, are computed as

$$\begin{aligned} N_{rr} &= T_{rr}\lambda_Z H = \frac{2aH\left(\beta\lambda_\Theta^2+1\right)\left[\lambda_R^4\left(\beta+\eta\lambda_\Theta^2\right)+\lambda_R^2\left(\beta\lambda_\Theta^2+1\right)-2\beta-\eta-1\right]}{\lambda_R\lambda_\Theta\left[\beta\lambda_\Theta^2+\lambda_R^2\left(\beta+\eta\lambda_\Theta^2\right)+1\right]}, \\ N_{\theta\theta} &= T_{\theta\theta}\lambda_Z H = \frac{2aH\left(\beta\lambda_R^2+1\right)\left[\lambda_\Theta^4\left(\beta+\eta\lambda_R^2\right)+\lambda_\Theta^2\left(\beta\lambda_R^2+1\right)-2\beta-\eta-1\right]}{\lambda_R\lambda_\Theta\left[\beta\lambda_\Theta^2+\lambda_R^2\left(\beta+\eta\lambda_\Theta^2\right)+1\right]}. \end{aligned} \tag{B.1}$$

The equilibrium equations are written as in Eq. (26) and the quantity $w=\varphi'_R$ is introduced, as was done in Sect. 3.1. The following system of differential equilibrium equations is obtained:

$$\begin{aligned} \lambda'_R &= \frac{\xi_0+\xi_1\lambda_\Theta+\xi_2\lambda_\Theta^2+\xi_3\lambda_\Theta^3+\xi_4\lambda_\Theta^4+\xi_5\lambda_\Theta^5+\xi_6\lambda_\Theta^6+\xi_7\lambda_\Theta^7}{R\lambda_\Theta\left(\beta\lambda_\Theta^2+1\right)\left[\zeta\lambda_R^2+2\lambda_R^4\left(\beta\lambda_\Theta^2+1\right)\left(\beta+\eta\lambda_\Theta^2\right)+\lambda_R^6\left(\beta+\eta\lambda_\Theta^2\right)^2+(2\beta+\eta+1)\left(\beta\lambda_\Theta^2+1\right)\right]}, \\ \lambda'_\Theta &= \frac{w-\lambda_\Theta}{R}, \\ w' &= \frac{\kappa_1\lambda'_R+\kappa_3\left[\lambda_R+\lambda_\Theta^2\lambda_R\left(\beta+\eta\lambda_R^2\right)+\beta\lambda_R^3\right]-2\lambda_R(2\beta+\eta+1)\left(\beta\lambda_R^2+1\right)\left(\lambda_R^2-w^2\right)}{2R\lambda_R\lambda_\Theta\left(\beta\lambda_\Theta^2+1\right)\left[\kappa_2+\lambda_R^2\lambda_\Theta^2\left(\beta+\eta\lambda_R^2\right)\right]}, \end{aligned} \tag{B.2}$$

where, for the sake of clarity, the following quantities were introduced:

$$\begin{aligned} \xi_0 &= -\lambda_R^5\left(2\beta^3w+\beta^2\eta w+\beta^2w\right)-\lambda_R^3\left(4\beta^2w+2\beta\eta w+2\beta w\right)-\lambda_R\left(2\beta w+\eta w+w\right), \\ \xi_1 &= -\beta^2\lambda_R^7-2\beta\lambda_R^5+\lambda_R^3\left(2\beta^2+\beta\eta+\beta-1\right)+\lambda_R\left(2\beta+\eta+1\right), \\ \xi_2 &= -w\beta^3\lambda_R^7-\lambda_R^5\left(2\beta^2\eta w+\beta^2w+\beta\eta^2w+\beta\eta w\right)+\lambda_R^3\left(2\beta^3w+\beta^2\eta w+\beta^2w-6\beta\eta w+\beta w-3\eta^2w-3\eta w\right) \\ &\quad -\lambda_R\left(2\beta^2w+\beta\eta w+\beta w-w\right), \\ \xi_3 &= \lambda_R^7\left(\beta^3-2\beta\eta\right)-2\eta\lambda_R^5-\lambda_R^3\left(2\beta^3+\beta^2\eta+\beta^2-6\beta\eta+\beta-3\eta^2-3\eta\right)+\lambda_R\left(4\beta^2+2\beta\eta+2\beta\right), \\ \xi_4 &= -2\beta^2\eta w\lambda_R^7-2\beta^3w\lambda_R^5+2\eta w\lambda_R^3+2\beta w\lambda_R, \\ \xi_5 &= \lambda_R^7\left(2\beta^2\eta-\eta^2\right)+2\beta^3\lambda_R^5+\lambda_R^3\left(2\beta^2\eta+\beta^2+\beta\eta^2+\beta\eta\right)+\lambda_R\left(2\beta^3+\beta^2\eta+\beta^2\right), \\ \xi_6 &= -w\beta\eta^2\lambda_R^7-\lambda_R^5\left(2\beta^2\eta w-\eta^2w\right)-\lambda_R^3\left(\beta^3w-2\beta\eta w\right)+\beta^2w\lambda_R, \\ \xi_7 &= \beta\eta^2\lambda_R^7+2\beta^2\eta\lambda_R^5+\beta^3\lambda_R^3, \qquad \zeta = \beta^2\lambda_\Theta^4+\lambda_\Theta^2\left[\beta\left(6\eta+2\right)+3\eta\left(\eta+1\right)\right]+3\beta\left(2\beta+\eta+1\right)+1, \\ \kappa_1 &= 2\beta Rw\lambda_R^2\lambda_\Theta^5\left(\beta+\eta\lambda_R^2\right)+2Rw\lambda_\Theta^3\left[\beta^2\left(\lambda_R^4-2\right)+\eta\lambda_R^4+\beta\left(2\lambda_R^2-\eta-1\right)\right]+2\kappa_2Rw\lambda_\Theta, \\ \kappa_2 &= \beta\lambda_R^4+\lambda_R^2-2\beta-\eta-1, \qquad \kappa_3 = \lambda_\Theta^2\left[2\beta\lambda_R^4-\lambda_R^2\left(\beta\sqrt{\lambda_R^2-w^2}+2\beta w^2-2\right)-2w^2\right]. \end{aligned} \tag{B.3}$$

The system of equilibrium equations Eq. (B.2) changed with respect to Eq. (29), which expresses the equilibrium for incompressible materials. However, its invariance property is preserved and the procedure to obtain the numerical solution can be still applied. Thus, the numerical solution of the TPBVP for compressible materials is obtained with the same procedure outlined in Sect. 3.1.

References

[1] L. R. G. Treloar, Strains in an inflated rubber sheet, and the mechanism of bursting, Rubber Chemistry and Technology 17 (4) (1944) 957–967.

[2] J. E. Adkins, R. S. Rivlin, Large elastic deformations of isotropic materials IX. the deformation of thin shells, Philosophical Transactions of the Royal Society of London. Series A, Mathematical and Physical Sciences 244 (888) (1952) 505–531.
[3] B. Gorissen, E. Milana, A. Baeyens, E. Broeders, J. Christiaens, K. Collin, D. Reynaerts, M. De Volder, Hardware sequencing of inflatable nonlinear actuators for autonomous soft robots, Advanced Materials 31 (3) (2019) 1804598.
[4] L. Chen, W. Chen, Y. Xue, M. Zhang, X. Chen, X. Cao, Z. Zhang, G. Li, T. Li, Investigation of the state transition and moving boundary in a pneumatic–hydraulic coupled dielectric elastomer actuator, Journal of Applied Mechanics 86 (3) (2019) 031004.
[5] J. Walker, T. Zidek, C. Harbel, S. Yoon, F. S. Strickland, S. Kumar, M. Shin, Soft robotics: a review of recent developments of pneumatic soft actuators, in: Actuators, Vol. 9, Multidisciplinary Digital Publishing Institute, 2020, p. 3.
[6] B. G. Stewart, S. K. Sitaraman, Biaxial inflation stretch test for flexible electronics, Advanced Engineering Materials (2021) 2001503.
[7] Z. Liu, A. McBride, B. L. Sharma, P. Steinmann, P. Saxena, Coupled electro-elastic deformation and instabilities of a toroidal membrane, Journal of the Mechanics and Physics of Solids 151 (2021) 104221.
[8] N. Goulbourne, E. Mockensturm, M. Frecker, A nonlinear model for dielectric elastomer membranes, Journal of Applied Mechanics 72 (6) (2005) 899–906.
[9] J. W. Fox, N. C. Goulbourne, On the dynamic electromechanical loading of dielectric elastomer membranes, Journal of the Mechanics and Physics of Solids 56 (8) (2008) 2669–2686.
[10] H. M. Wang, Viscoelastic analysis of a spring-connected dielectric elastomer actuator undergoing large inhomogeneous deformation, International Journal of Mechanical Sciences 136 (2018) 17–23.
[11] T. Hiruta, N. Hosoya, S. Maeda, I. Kajiwara, Experimental validation of vibration control in membrane structures using dielectric elastomer actuators in a vacuum environment, International Journal of Mechanical Sciences 191 (2021) 106049.
[12] Y. X. Xie, J. C. Liu, Y. B. Fu, Bifurcation of a dielectric elastomer balloon under pressurized inflation and electric actuation, International Journal of Solids and Structures 78 (2016) 182–188.
[13] C. Grosjean, G. B. Lee, W. Hong, Y. C. Tai, C. M. Ho, Micro balloon actuators for aerodynamic control, in: Proceedings MEMS 98. IEEE. Eleventh Annual International Workshop on Micro Electro Mechanical Systems. An Investigation of Micro Structures, Sensors, Actuators, Machines and Systems. Cat. No. 98CH36176, IEEE, 1998, pp. 166–171.
[14] W. Cheng, M. J. Campolongo, S. J. Tan, D. Luo, Freestanding ultrathin nano-membranes via self-assembly, Nano Today 4 (6) (2009) 482–493.
[15] A. Pacheco-Sanjuán, R. Batra, Accuracy of Föppl–von Karman membrane theory for determining elastic constants of monolayer graphene, International Journal of Mechanical Sciences 163 (2019) 105154.
[16] A. Wineman, D. Wilson, J. W. Melvin, Material identification of soft tissue using membrane inflation, Journal of Biomechanics 12 (11) (1979) 841–850.
[17] E. R. Serina, E. Mockensturm, C. D. Mote Jr, D. Rempel, A structural model of the forced compression of the fingertip pulp, Journal of Biomechanics 31 (7) (1998) 639–646.
[18] M. Gil Pérez, T. H. K. Kang, I. Sin, S. D. Kim, Nonlinear analysis and design of membrane fabric structures: modeling procedure and case studies, Journal of Structural Engineering 142 (11) (2016) 05016001.
[19] S. Gale, W. J. Lewis, Patterning of tensile fabric structures with a discrete element model using dynamic relaxation, Computers & Structures 169 (2016) 112–121.
[20] W. V. Jones, Evolution of scientific ballooning and its impact on astrophysics research, Advances in Space Research 53 (10) (2014) 1405–1414.
[21] R. Glaser, Multi-objective characterization of an inflatable space structure with a quasi-static experimental deflation and finite element analysis, International Journal of Mechanical Sciences 205 (2021) 106614.
[22] C. K. Hirwani, S. K. Panda, P. K. Mishra, Influence of debonding on nonlinear deflection responses of curved composite panel structure under hygro-thermo-mechanical loading–macro-mechanical FE approach, International Journal of Non-Linear Mechanics 128 (2021) 103636.
[23] N. Sharma, A. K. Lalepalli, C. K. Hirwani, A. Das, S. K. Panda, U. Topal, T. Dede, Optimal deflection and stacking sequence prediction of curved composite structure using hybrid (FEM and soft computing) technique, Engineering with Computers 37 (1) (2021) 477–487.
[24] P. V. Katariya, C. K. Hirwani, S. K. Panda, Geometrically nonlinear deflection and stress analysis of skew sandwich shell panel using higher-order theory, Engineering with Computers 35 (2) (2019) 467–485.
[25] D. Shinde, P. V. Katariya, K. Mehar, M. R. Khan, S. K. Panda, H. K. Pandey, Experimental training of shape memory alloy fibres under combined thermomechanical loading, Structural Engineering and Mechanics, An Int'l Journal 68 (5) (2018) 519–526.
[26] S. S. Sahoo, S. K. Panda, V. K. Singh, Experimental and numerical investigation of static and free vibration responses of woven glass/epoxy laminated composite plate, Proceedings of the Institution of Mechanical Engineers, Part L: Journal of Materials: Design and Applications 231 (5) (2017) 463–478.
[27] S. S. Sahoo, V. K. Singh, S. K. Panda, Nonlinear flexural analysis of shallow carbon/epoxy laminated composite curved panels: experimental and numerical investigation, Journal of Engineering Mechanics 142 (4) (2016) 04016008.
[28] W. B. Fichter, Some solutions for the large deflections of uniformly loaded circular membranes, Vol. 3658, National Aeronautics and Space Administration, Langley Research Center, 1997.
[29] W. H. Yang, W. W. Feng, On axisymmetrical deformations of nonlinear membranes, Journal of Applied Mechanics 37 (4) (1970) 1002–1011.
[30] A. Patil, A. DasGupta, Finite inflation of an initially stretched hyperelastic circular membrane, European Journal of Mechanics-A/Solids 41 (2013) 28–36.
[31] A. Chaudhuri, A. DasGupta, On the static and dynamic analysis of inflated hyperelastic circular membranes, Journal of

the Mechanics and Physics of Solids 64 (2014) 302–315.
[32] M. X. Liu, C. G. Wang, X. D. Li, Rigid-flexible contact analysis of an inflated membrane balloon with various contact conditions, International Journal of Solids and Structures 144 (2018) 218–229.
[33] A. Patil, A. DasGupta, A. Eriksson, Contact mechanics of a circular membrane inflated against a deformable substrate, International Journal of Solids and Structures 67 (2015) 250–262.
[34] A. S. Wineman, H. E. Huntley, Numerical simulation of the effect of damaged induced softening on the inflation of a circular rubber membrane, International Journal of Solids and Structures 31 (23) (1994) 3295–3313.
[35] J. C. Selby, M. A. Shannon, Inflation of a circular elastomeric membrane into a horizontally semi-infinite liquid reservoir of finite vertical depth: Quasi-static deformation model, International Journal of Engineering Science 47 (5-6) (2009) 700–717.
[36] G. Tamadapu, A. DasGupta, Effect of curvature and anisotropy on the finite inflation of a hyperelastic toroidal membrane, European Journal of Mechanics-A/Solids 46 (2014) 106–114.
[37] S. Roychowdhury, A. DasGupta, Symmetry breaking during inflation of a toroidal membrane, Journal of the Mechanics and Physics of Solids 121 (2018) 328–340.
[38] C. Zhang, L. Fan, Y. Tan, Sequential limit analysis for clamped circular membranes involving large deformation subjected to pressure load, International Journal of Mechanical Sciences 155 (2019) 440–449.
[39] C. Y. Wang, Inflating and deflating an underwater cylindrical membrane structure, European Journal of Mechanics-A/Solids 85 (2021) 104127.
[40] N. H. Reddy, P. Saxena, Limit points in the free inflation of a magnetoelastic toroidal membrane, International Journal of Non-Linear Mechanics 95 (2017) 248–263.
[41] M. Soleimani, W. R. J. Funnell, Deformation and stability of short cylindrical membranes, International Journal of Mechanical Sciences 119 (2016) 266–272.
[42] Y. Li, J. A. Nemes, A. A. Derdouri, Membrane inflation of polymeric materials: Experiments and finite element simulations, Polymer Engineering & Science 41 (8) (2001) 1399–1412.
[43] D. C. Pamplona, P. B. Goncalves, S. R. X. Lopes, Finite deformations of cylindrical membrane under internal pressure, International Journal of Mechanical Sciences 48 (6) (2006) 683–696.
[44] R. Österlöf, H. Wentzel, L. Kari, An efficient method for obtaining the hyperelastic properties of filled elastomers in finite strain applications, Polymer testing 41 (2015) 44–54.
[45] M. Pelliciari, D. P. Pasca, A. Aloisio, A. M. Tarantino, Size effect in single layer graphene sheets and transition from molecular mechanics to continuum theory, International Journal of Mechanical Sciences 214 (2022) 106895.
[46] L. Zhou, S. Wang, L. Li, Y. Fu, An evaluation of the Gent and Gent-Gent material models using inflation of a plane membrane, International Journal of Mechanical Sciences 146 (2018) 39–48.
[47] M. Coelho, D. Roehl, K. U. Bletzinger, Numerical and analytical solutions with finite strains for circular inflated membranes considering pressure–volume coupling, International Journal of Mechanical Sciences 82 (2014) 122–130.
[48] J. Yuan, X. Liu, H. Xia, Y. Huang, Analytical solutions for inflation of pre-stretched elastomeric circular membranes under uniform pressure, Theoretical and Applied Mechanics Letters (2021) 100243.
[49] X. Yang, L. Yu, R. Long, Contact mechanics of inflated circular membrane under large deformation: Analytical solutions, International Journal of Solids and Structures 233 (2021) 111222.
[50] L. Lanzoni, A. M. Tarantino, Large nonuniform bending of beams with compressible stored energy functions of polynomial-type, International Journal of Mechanical Sciences 196 (2021) 106287.
[51] M. Sasso, G. Palmieri, G. Chiappini, D. Amodio, Characterization of hyperelastic rubber-like materials by biaxial and uniaxial stretching tests based on optical methods, Polymer Testing 27 (8) (2008) 995–1004.
[52] N. Kumar, V. V. Rao, Hyperelastic Mooney-Rivlin model: Determination and physical interpretation of material constants, Parameters 2 (10) (2016) 01.
[53] M. Pelliciari, A. M. Tarantino, Equilibrium and stability of anisotropic hyperelastic graphene membranes, Journal of Elasticity 144 (2021) 169–195.
[54] M. Pelliciari, A. M. Tarantino, A nonlinear molecular mechanics model for graphene subjected to large in-plane deformations, International Journal of Engineering Science 167 (2021) 103527.
[55] L. Lanzoni, A. M. Tarantino, Finite anticlastic bending of hyperelastic solids and beams, Journal of Elasticity 131 (2) (2018) 137–170.
[56] M. Pelliciari, A. M. Tarantino, Equilibrium paths for von Mises trusses in finite elasticity, Journal of Elasticity 138 (2) (2020) 145–168.
[57] A. P. S. Selvadurai, Deflections of a rubber membrane, Journal of the Mechanics and Physics of Solids 54 (6) (2006) 1093–1119.
[58] G. Marckmann, E. Verron, Comparison of hyperelastic models for rubber-like materials, Rubber chemistry and technology 79 (5) (2006) 835–858.
[59] R. M. Soares, P. B. Gonçalves, Large-amplitude nonlinear vibrations of a Mooney–Rivlin rectangular membrane, Journal of Sound and Vibration 333 (13) (2014) 2920–2935.
[60] T. Gopesh, J. Friend, Facile analytical extraction of the hyperelastic constants for the two-parameter Mooney–Rivlin model from experiments on soft polymers, Soft Robotics 8 (4) (2021) 365–370.
[61] V. P. W. Shim, L. M. Yang, C. T. Lim, P. H. Law, A visco-hyperelastic constitutive model to characterize both tensile and compressive behavior of rubber, Journal of Applied Polymer Science 92 (1) (2004) 523–531.
[62] H. O. Foster, Very large deformations of axially symmetrical membranes made of neo-Hookean materials, International Journal of Engineering Science 5 (1) (1967) 95–117.
[63] L. Lanzoni, A. M. Tarantino, Equilibrium configurations and stability of a damaged body under uniaxial tractions,

Zeitschrift für angewandte Mathematik und Physik 66 (1) (2015) 171–190.
[64] D. Steck, J. Qu, S. B. Kordmahale, D. Tscharnuter, A. Muliana, J. Kameoka, Mechanical responses of Ecoflex silicone rubber: Compressible and incompressible behaviors, Journal of Applied Polymer Science 136 (5) (2019) 47025.
[65] R. W. Ogden, Large deformation isotropic elasticity–on the correlation of theory and experiment for incompressible rubberlike solids, Proceedings of the Royal Society of London. A. Mathematical and Physical Sciences 326 (1567) (1972) 565–584.
[66] O. H. Yeoh, Characterization of elastic properties of carbon-black-filled rubber vulcanizates, Rubber chemistry and technology 63 (5) (1990) 792–805.